Paradigm International Journal of Mathematics and Computer in Engineering 4(2) (2026) 293–320

International Journal of Mathematics and Computer in Engineering

https://reference-global.com/journal/IJMCE

Original Study

Dynamics of solitons, multi-lumps, and their interactions of the Konopelchenko-Dubrovsky-Kaup-Kupershmidt and Bogoyavlensky-Konopelchenko model in (3+1)-dimensions using the modern advanced approach

Sachin Kumar[1] †, Jaionto Karmokar[1,2]

[1]Department of Mathematics, Faculty of Mathematical Sciences, University of Delhi, Delhi, 110007, India

[2]Department of Computer Science and Mathematics, Bangladesh Agricultural University, Mymensingh, 2202, Bangladesh

Communicated by Haci Mehmet Baskonus; Received: 02.10.2025; Accepted: 27.02.2026; Online: 00.00.2026

Abstract

In this original research, we explore new forms of soliton solutions, lumps, and the dynamics of water waves of the considered Generalized Konopelchenko-Dubrovsky-Kaup-Kupershmidt (KDKK) and Bogoyavlensky-Konopelchenko (BK) equations in (3+1)-dimensions, utilizing the Hirota bilinear approach. We apply the Painlevé analysis to check the integrability of this model. We formulate a bilinear equation in an auxiliary function using the Cole-Hopf transformation and then develop it into a Hirota bilinear form using a bilinear differential operator. Based on this technique, we derive lump waves, breaking phenomena, solitons, peakons, wave interactions, and wave-to-wave collisions. The solutions are obtained using ansatz functions in quadratic, sine, cosine, and exponential functions. We also illustrate how the lump interacts with solitary, periodic, and breather waves to generate various dynamics of water waves in the obtained solutions, which are visualized graphically via 2D, 3D, and contour plots with the help of symbolic software Maple. We also show the phase plane portraits, bifurcation analysis, and sensitivity analysis based on the bifurcation method with the help of the equilibrium points of the governing model studied.

Keywords: Analytical solutions, KDKK and BK model, Painlevé analysis, Hirota bilinear method, solitons, symbolic computation work.
AMS 2020 codes: 35A24; 35B32; 35C05; 35C07; 35C08.

1 Introduction

Nonlinear evolution equations (NLEEs) are commonly used in numerous fields, including soliton theory, nonlinear dynamics, plasma physics, condensed matter physics, optical physics, and fluid dynamics, because most natural systems exhibit nonlinear behavior. In the context of fluid dynamics, these equations describe the evolution of water waves under different heights and pressures. In plasma physics and quantum field theory, NLEEs account for the interactions between particle and wave dispersion, particularly when quantum molecules do not behave linearly across all scales [1–4]. In nonlinear sciences, soliton theory is the most significant and efficient way for finding lump solutions, also known as analytical rational function solutions [5]. Nonlinear

†Corresponding author.
Email address: sachinambariya@gmail.com

Paradigm
ISSN 2956-7068 doi:10.2478/ijmce-2026-0017 Paradigm

partial differential equations involve numerous boundary conditions, expansion, and dispersion terms; these terms often interact with each other, making it difficult to understand the results of the problem. According to Yu and et al. [6], the most significant component of a single wave is the lump wave, which has several characteristics. Manakov and et al. [7] introduced the most basic lump wave solution to the KP equation for two-dimensional soliton solutions in 1977. However, various scientific disciplines have studied lump wave solutions, including oceanography [8], shallow water waves [9], atmospheric [10], nonlinear optics [11], and many more. To generate lump solutions, several efficient techniques have been proposed, including the parameter limit method [12], the bilinear neural network method [13], the Hirota bilinear method [14,15], the Painlevé analysis [16], the Darboux transformation [17,18], and many more. These techniques can help to understand and evaluate different solutions to nonlinear partial differential equations (NPDEs).

Recently, Yang [14] investigated the resonant interaction between 2-solitons and 3-solitons and obtained X-, Y-, and double-X-shaped solitons. Feng and Zhao [19] searched for a suitable expression for the lump solution over the entire plane for a generalized (3+1)-dimensional NPDE. Chen and et al. [20] achieved the lump and breather solutions, as well as their interactions, for the generalized CH-KP equation in hydrodynamics and ocean physics. Ma and et al. [21] employed the Hirota bilinear technique to find the lump solutions of (2+1)-dimensional combined nonlinear equations. Wang and et al. [22] used the symbolic computations to determine solutions to nonlinear wave equations for fluids containing gas bubbles, including lump waves, rogue wave-solitary waves, and mixed lump-solitary waves. Moreover, Yang and Ma [23] applied the Hirota bilinear technique to generate lump solutions for the (2+1)-dimensional BKP equation. He and et al. [24] have investigated the (2+1)-dimensional BLMP and Ito equations for the interaction between lumps and multi-solitons using direct techniques. Ma and Zhou [5] introduced the quadratic function method to generate lump solutions for NPDEs. Using the quadratic function method, Zhou and et al. [25] obtained lump solutions to the (3+1)-dimensional generalized CBS equation. Inspired by Hirota's direct technique, we focus on lump soliton solutions and their collisions by combining quadratic functions with trigonometric and exponential functions.

In this study, we investigate a (3+1)-dimensional generalized NPDEs, also known as the KDKK and BK equations introduced by Feng and Zhao [19], as follows:

$$\kappa_1\frac{\partial u}{\partial t}+\kappa_2\left(\frac{\partial^3 u}{\partial x^2\partial z}+3u\frac{\partial u}{\partial z}+3\frac{\partial u}{\partial x}\partial^{-1}u_z\right)+\kappa_3\left(\frac{\partial^3 u}{\partial x^2\partial y}+3u\frac{\partial u}{\partial y}+3\frac{\partial u}{\partial x}\partial^{-1}u_y\right)+\kappa_4\frac{\partial u}{\partial x}+\kappa_5\frac{\partial u}{\partial y}+\kappa_6\frac{\partial u}{\partial z}=0, \tag{1}$$

where $\partial^{-1}u_z=\int\frac{\partial u}{\partial z}dx$, $\partial^{-1}u_y=\int\frac{\partial u}{\partial y}dx$, and κ_i $(1\le i\le 6)$ are nonzero real constants. The presence of constant and free parameters is crucial for determining the exact solution of equation (1). Table 1 presents the generalized well-known equations derived from equation (1) by variation of κ_i.

The purpose of this research is to present novel insights into the collision of waves, such as lump, periodic, solitary, and breather waves in a generalized KDKK and BK equations through the Hirota bilinear technique. The motivation behind this technique has several advantages. First, this method is a very efficient, accurate, reliable, and sophisticated way to determine the exact solution of the NPDEs. Second, this method does not require inverse scattering integration, which makes it easier to depict soliton solutions. Third, this method is the easiest to handle algebraically because it transforms the governing NPDEs into a bilinear form. Finally, once the bilinear form is known, it provides a systematic technique that can often be used to solve for N-soliton solutions.

In addition, we introduce the analysis of bifurcation and equilibrium states by considering a travelling wave transformation of the governing equation to obtain a 2D planar dynamical structure. The solution to the system is related to the Hamiltonian function, which is shown in the figure.

Table 1 Particular cases of equation (1) found in ocean dynamics and related fields.

Variation of κ_i	**PDEs**	**Special form**
$\kappa_1 = \kappa_2 = 1$, $\kappa_3 = \kappa_4 = \kappa_5 = \kappa_6 = 0$, $z = x$	$u_t + u_{xxx} + 6uu_x = 0$	KdV equation [26]
$\kappa_1 = 1$, $\kappa_2 = a_1$, $\kappa_3 = a_5$, $\kappa_5 = 0$, $\kappa_4 + \kappa_6 = 0$, $z = x$	$u_t + a_1 u_{xxx} + \frac{1}{2}a_2(u^2)_x + a_3 u_{xxxxx}$ $+a_4 v_y + a_5 u_{xxy} + a_6(u_x v + u v_x)$ $+a_7(uu_{xx})_x + \frac{1}{3}a_8(u^3)_x = 0$, $v_x = u_y$, for $a_2 = 6a_1$, $a_6 = 3a_5$, $a_3 = a_4 = a_7 = a_8 = 0$	(2+1)-D gKDKK equation [27]
$\kappa_1 = 1$, $\kappa_2 = b_1$, $\kappa_3 = b_2$, $\kappa_4 = b_3$, $\kappa_5 = b_4$, $\kappa_6 = 0$, $b_5 = 0, z = x$	$u_t + 6b_1(uu_x + \frac{1}{6}u_{xxx})$ $+3b_2(\frac{1}{3}u_{xxy} + uu_y + u_x v_y)$ $+b_3 u_x + b_4 u_y + b_5 v_{yy} = 0$, $v_x = u$	(2+1)-D gBK equation [28]

The Hamiltonian system is constructed more specifically using Galilean transformations, which emphasize the system's periodic and chaotic behavior [29–32]. For a given parameter, a dynamical system can exhibit the phenomenon of multistability, which consists of multiple distinct dynamical behaviors under different initial conditions [32, 33]. Sensitivity analysis makes it easier to understand how a dynamic system behaves under different initial conditions.

To the best of our knowledge, equation (1) has not been studied in the context of collisions between periodic and lump waves, collisions between single-lump and solitary waves, or collisions between lump and breather waves. Furthermore, this equation has never been investigated through bifurcation analysis, equilibrium conditions, and sensitivity analysis. This article fills this gap by using a bifurcation-based approach to analyze soliton interaction, water wave dynamics, the effect of wind on equilibrium structures, stability, and soliton dynamics. It has special significance due to the enhanced physical formulation of the KDKK and BK equations, as well as the methodological innovation of applying bifurcation and sensitivity analysis. This combination provides a new understanding of how external attraction and dissipation affect nonlinear wave dynamics.

This paper is outlined as follows: In Section 2, the Painlevé test is employed to examine the integrability of equation (1). Section 3 discusses the proposed method. Section 4 explores the wave-to-wave collision structures and their solutions using different ansatz functions. Section 5 presents the physical interpretation of the findings. Section 6 discusses the equilibrium state and bifurcation analysis of a dynamic system, which shows the phase portrait and Hamiltonian function graphics. Section 7 covers the sensitivity analysis of a dynamic system for different initial conditions. Finally, the findings are summarized and presented as a conclusion in Section 8.

2 Painlevé analysis

This section provides an outline of the Painlevé test, which is an effective technique for checking whether a nonlinear PDE can be solved in an integrable manner [34, 35]. If a nonlinear system passes the Painlevé test, that is, if each movable singular point of the solutions is a simple pole, then it is deemed integrable. Weiss and et al. [36] developed this technique to check the integrability of nonlinear PDEs by examining the integrability

criteria. This process is described in three steps: first, the behavior of the leading-order is examined; second, the resonances are identified; and third, the conditions at the resonance points are verified.

We assume that the field u in equation (1) is expanded in a Laurent series about the singular manifold $h(x,y,z,t)=0$, to perform the integrability test as

$$u(x,y,z,t)=\sum_{q=0}^{\infty} u_q h^{q+\Omega}, \tag{2}$$

where Ω is an integer and $u_q = u_q(x,y,z,t)$; $q = 0,1,2,\cdots$ are arbitrary functions, respectively.
Substituting equation (2) into equation (1) through a leading-order analysis based on the dominant terms, we get

$$\Omega = -2, \quad u_0 = -2h_x^2.$$

Next, to obtain resonance, we take

$$u = u_0 h^{-2} + u_q h^{q-2}.$$

Substituting these into equation (1) and collecting the coefficients of the dominant terms gives the characteristic relationship for resonance, which is:

$$\Big((q-2)(q-3)(q-4)-12(q-4)\Big)h_x^2(\kappa_2 h_z+\kappa_3 h_y)=0. \tag{3}$$

Since $h(x,y,z,t)$ and its derivatives are not equal to zero, the resonances of equation (1) are

$$q = -1, \quad 4, \quad 6.$$

The resonance $q=-1$ indicates the random selection of the singular manifold $h(x,y,z,t)=0$. The explicit expression for u_q indicates the existence of sufficient arbitrary functions for $q=4$ and $q=6$ resonances. The condition of compatibility is fulfilled by positive resonance. Therefore, the tested KDKK and BK equations (1) pass the Painlevé test for integrability.

3 Hirota's bilinear form of the governing equation

Suppose Ψ_i is the phase of equation (1), such that

$$\Psi_i = \alpha_i x + \beta_i y + \gamma_i z - \delta_i t + \vartheta_i, \tag{4}$$

where α_i, β_i, γ_i, and ϑ_i are real parameters. By substituting $u = e^{\Psi_i}$ into equation (1) and considering the linear terms, we determine that the dispersion δ_i is

$$\delta_i = \frac{\beta_i\alpha_i^2\kappa_3+\alpha_i^2\gamma_i\kappa_2+\beta_i\kappa_5+\alpha_i\kappa_4+\gamma_i\kappa_6}{\kappa_1}. \tag{5}$$

Now, consider a logarithmic transformation (also known as the Cole-Hopf transformation) for the dependent variable $u = u(x,y,z,t)$ as

$$u = \frac{\partial^2}{\partial x^2}(2\ln f). \tag{6}$$

Let $f = f(x,y,z,t)$ be an auxiliary function, and rewrite equation (6) in another form as follows:

$$u = V_{xx}, \quad V = 2\ln f. \tag{7}$$

Substituting equation (7) into equation (1) and integrating with respect to x, we get

$$\kappa_1 V_{xt} + \kappa_2 (3V_{xx}V_{xz} + V_{xxxz}) + \kappa_3 (3V_{xx}V_{xy} + V_{xxxy}) + \kappa_4 V_{xx} + \kappa_5 V_{xy} + \kappa_6 V_{xz} = 0. \tag{8}$$

Substituting the derivatives of the second term of equation (7) into equation (8), we get

$$\begin{aligned} &\kappa_1 (2ff_{tx} - 2f_t f_x) + \kappa_2 (2ff_{xxxz} - 6f_x f_{xxz} + 6f_{xx}f_{xz} - 2f_{xxx}f_z) + \\ &\kappa_3 (2ff_{xxxy} - 6f_x f_{xxy} + 6f_{xx}f_{xy} - 2f_{xxx}f_y) + \kappa_4 \left(2ff_{xx} - 2f_x^2\right) + \\ &\kappa_5 (2ff_{xy} - 2f_x f_y) + \kappa_6 (2ff_{xz} - 2f_x f_z) = 0. \end{aligned} \tag{9}$$

This equation represents a bilinear equation that is transformed into Hirota bilinear form using a bilinear differential operator. Hirota [15] designed the bilinear differential operator D_r, where $r = x, y, z, t$. It can be expressed as

$$\begin{aligned} D_x^{p_1} D_y^{p_2} D_z^{p_3} D_t^{p_4} M \cdot N = &\left(\frac{\partial}{\partial x} - \frac{\partial}{\partial x'}\right)^{p_1} \left(\frac{\partial}{\partial y} - \frac{\partial}{\partial y'}\right)^{p_2} \left(\frac{\partial}{\partial z} - \frac{\partial}{\partial z'}\right)^{p_3} \left(\frac{\partial}{\partial t} - \frac{\partial}{\partial t'}\right)^{p_4} \\ &M(x,y,z,t) N(x',y',z',t')\big|_{x'=x,\ y'=y,\ z'=z,\ t'=t}, \end{aligned}$$

where p_1, p_2, p_3, p_4 are positive integers and x', y', z', t' are formal variables. Using this definition of the D-operator, we obtain the necessary operators, such as

$$\begin{aligned} D_x D_j f \cdot f &= 2(ff_{xj} - f_x f_j); j = y, z, t, \\ D_x^2 f \cdot f &= 2(ff_{xx} - f_x^2), \\ D_x^3 D_j f \cdot f &= 2(ff_{xxxj} - 3f_x f_{xxj} + 3f_{xx}f_{xj} - f_{xxx}f_j); j = y, z. \end{aligned} \tag{10}$$

Therefore, the bilinear form of equation (9) is

$$\left[\kappa_1 D_x D_t + \kappa_2 D_x^3 D_z + \kappa_3 D_x^3 D_y + \kappa_4 D_x^2 + \kappa_5 D_x D_y + \kappa_6 D_x D_z\right] f \cdot f = 0. \tag{11}$$

Therefore, if the auxiliary function f satisfies equation (11), then equation (6) will be considered as a solution of KDKK and BK equations (1). In the following section, we investigate an expression for an ansatz function that leads to the general solutions for solitary waves, breather waves, lump waves, periodic waves, and their collisions in detail.

4 Wave-to-wave collisions with different ansatz functions and their solutions

4.1 Lump wave solutions of KDKK and BK equations

An expression for the auxiliary function f is considered to find the lump wave solution of the KDKK and BK equations (1):

$$f = (l_1 x + m_1 y + n_1 z + w_1 t + \delta_1)^2 + (l_2 x + m_2 y + n_2 z + w_2 t + \delta_2)^2 + \eta, \tag{12}$$

where l_1, l_2, m_1, m_2, n_1, n_2, w_1, w_2, δ_1, δ_2, and η are free parameters to be determined later. Substituting equation (12) into equation (11) and equating all the coefficients of x, y, z, t, and their multiples equal to zero. Then, a system of algebraic equations consisting of l_1, l_2, m_1, m_2, n_1, n_2, w_1, w_2, δ_1, δ_2, and η is obtained. By solving the system of equations using symbolic software Maple, we obtain the values of some parameters:

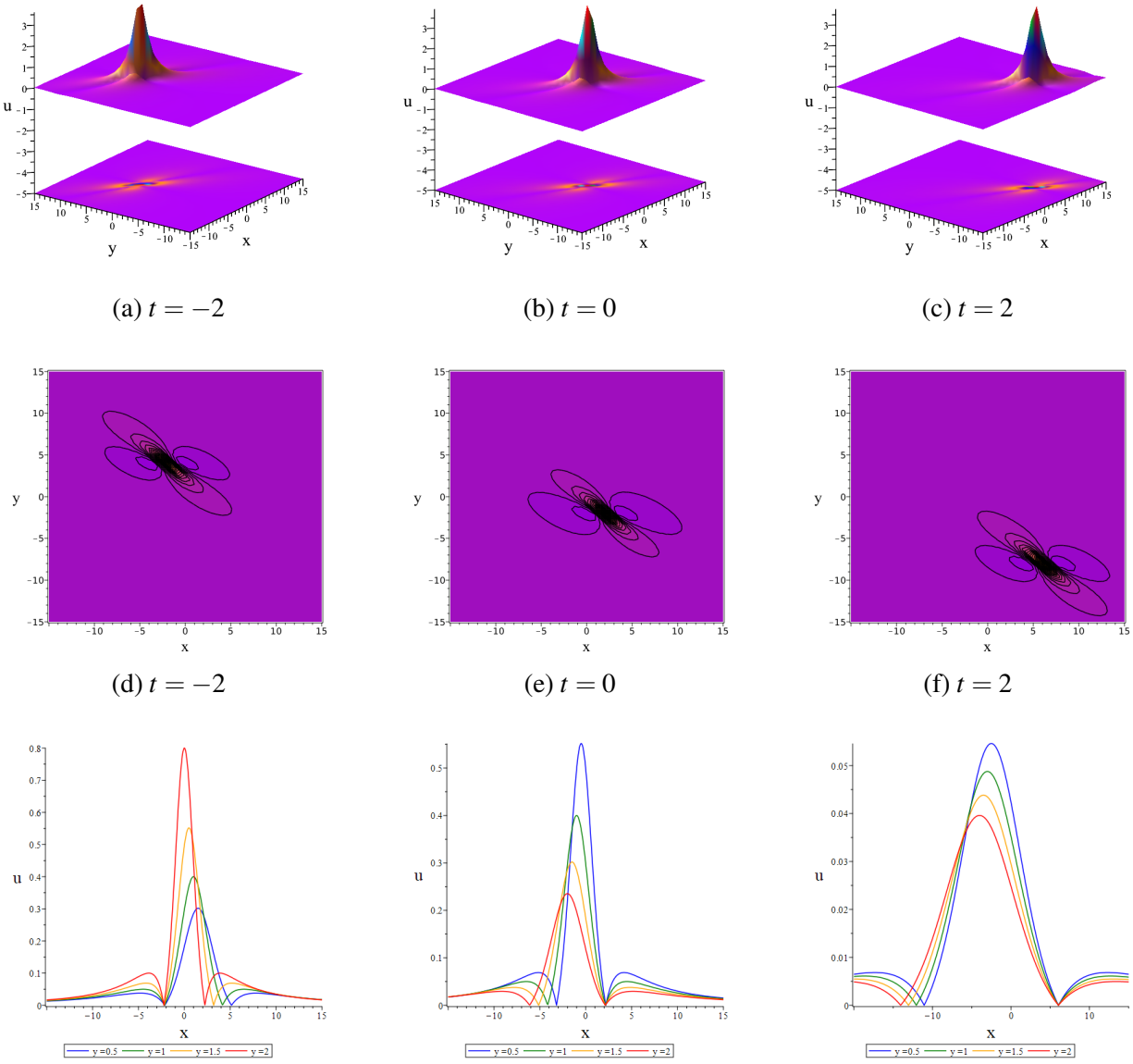

Fig. 1 Wave profiles of the lump wave solution for equation (15): **(a)-(c)** are the 3D profiles with density plots; **(d)-(f)** are the contour plots; and **(g)-(i)** are the wave propagation along the x-axis.

Case I.

$$l_2=0, m_1=-\frac{\kappa_2\left(w_1\kappa_1+l_1\kappa_4\right)}{\kappa_2\kappa_5-\kappa_3\kappa_6}, n_1=\frac{\kappa_3\left(w_1\kappa_1+l_1\kappa_4\right)}{\kappa_2\kappa_5-\kappa_3\kappa_6}, w_2=-\frac{m_2\kappa_5+n_2\kappa_6}{\kappa_1}. \tag{13}$$

Substituting the parameter values of equation (13) into equation (12), we attain

$$\begin{aligned} f=&\left(l_1x-\frac{\kappa_2\left(l_1\kappa_4+w_1\kappa_1\right)y}{\kappa_2\kappa_5-\kappa_3\kappa_6}+\frac{\kappa_3\left(l_1\kappa_4+w_1\kappa_1\right)z}{\kappa_2\kappa_5-\kappa_3\kappa_6}+w_1t+\delta_1\right)^2+\\ &\left(m_2y+n_2z-\frac{t\left(m_2\kappa_5+n_2\kappa_6\right)}{\kappa_1}+\delta_2\right)^2+\eta. \end{aligned} \tag{14}$$

Substituting the expression (14) into equation (6) yields the appropriate solutions to the KDKK and BK equations (1), which represent the lump-type wave solution. Choosing the particular value of the free parameters: $l_1 = 1$, $w_1 = 1$, $m_2 = 1$, $n_2 = 1$, $\delta_1 = 1$, $\delta_2 = 1$, $\kappa_1 = 1$, $\kappa_2 = 1$, $\kappa_3 = 1$, $\kappa_4 = -2$, $\kappa_5 = -1$, $\kappa_6 = -2$, and $\eta = 1$. Then, the solutions are calculated and simplified. Finally, we obtain the specific lump wave solution of the governing equation (1) is

$$u = \frac{4\left(-x^2+8t^2-2xy+2xz-2xt+4yt+8zt+4yz-2x+4z+4t+1\right)}{\left(x^2+2y^2+2z^2+10t^2+2xy-2xz+2xt+8yt+4zt+2x+4y+8t+3\right)^2}. \tag{15}$$

The wave profiles of the lump wave solutions of equation (15) are shown in Fig.1 through contour plots, 2D, and 3D profiles.

Case II.

$$\begin{aligned} m_1 &= -\frac{l_1\kappa_4+n_1\kappa_6+w_1\kappa_1}{\kappa_5}, \\ m_2 &= -\frac{\kappa_3\kappa_4\kappa_6 l_1^2-\kappa_2\kappa_5\kappa_6 l_1 n_1+\kappa_3\kappa_6^2 l_1 n_1+\kappa_1\kappa_3\kappa_6 l_1 w_1+\kappa_2\kappa_4\kappa_5 l_2^2+\kappa_1\kappa_2\kappa_5 l_2 w_2}{\kappa_5 l_2\left(\kappa_2\kappa_5-\kappa_3\kappa_6\right)}, \\ n_2 &= \frac{\kappa_3\kappa_4 l_1^2-\kappa_2\kappa_5 l_1 n_1+\kappa_3\kappa_6 n_1 l_1+\kappa_1\kappa_3 l_1 w_1+\kappa_3\kappa_4 l_2^2+\kappa_1\kappa_3 w_2 l_2}{\left(\kappa_2\kappa_5-\kappa_3\kappa_6\right) l_2}. \end{aligned} \tag{16}$$

Substituting the parameter values of equation (16) into equation (12), we attain

$$\begin{aligned} f = &\left(l_1 x-\frac{\left(l_1\kappa_4+n_1\kappa_6+w_1\kappa_1\right)y}{\kappa_5}+n_1 z+w_1 t+\delta_1\right)^2+ \\ &\left(l_2 x-\frac{\left(\kappa_3\kappa_4\kappa_6 l_1^2-\kappa_2\kappa_5\kappa_6 l_1 n_1+\kappa_3\kappa_6^2 l_1 n_1+\kappa_1\kappa_3\kappa_6 l_1 w_1+\kappa_2\kappa_4\kappa_5 l_2^2+\kappa_1\kappa_2\kappa_5 l_2 w_2\right)y}{\kappa_5 l_2\left(\kappa_2\kappa_5-\kappa_3\kappa_6\right)}+\right. \\ &\left.\frac{\left(\kappa_3\kappa_4 l_1^2-\kappa_2\kappa_5 l_1 n_1+\kappa_3\kappa_6 n_1 l_1+\kappa_1\kappa_3 l_1 w_1+\kappa_3\kappa_4 l_2^2+\kappa_1\kappa_3 w_2 l_2\right)z}{\left(\kappa_2\kappa_5-\kappa_3\kappa_6\right) l_2}+w_2 t+\delta_2\right)^2+\eta. \end{aligned} \tag{17}$$

Substituting the expression (17) into equation (6) yields the appropriate solutions to the KDKK and BK equations (1), which represent the lump-type wave solution. Choosing the particular value of the free parameters: $l_1 = 1$, $n_1 = 1$, $w_1 = 1$, $l_2 = 1$, $w_2 = 1$, $\delta_1 = -1$, $\delta_2 = 1$, $\eta = 1$, $\kappa_1 = 2$, $\kappa_2 = 2$, $\kappa_3 = 1$, $\kappa_4 = -2$, $\kappa_5 = -1$, and $\kappa_6 = 1$. Then, the solutions are calculated and simplified. Finally, we obtain the specific lump wave solution of the governing equation (1) is

$$u = -\frac{8\left(2x^2-2y^2-2z^2+2t^2+4xt-4yz+4y+4z-3\right)}{\left(2x^2+2y^2+2z^2+2t^2+4xt+4yz-4y-4z+3\right)^2}. \tag{18}$$

In Fig. 2, the wave profiles of the lump wave solutions of equation (18) are shown for different values of z through contour plots, 2D, and 3D profiles.

4.2 Collision of waves: single-lump wave and solitary wave

Consider a function that combines quadratic and exponential functions to examine the effect of a collision between a single lump and a solitary wave on the governing equation (1). For example,

$$f = (l_1 x+m_1 y+n_1 z+w_1 t+\delta_1)^2+(l_2 x+m_2 y+n_2 z+w_2 t+\delta_2)^2+exp(l_3 x+m_3 y+n_3 z+w_3 t)+\eta, \tag{19}$$

where l_r, m_r, n_r, w_r, δ_1, δ_2, and η are free parameters with $r = 1,2,3$ to be determined. Substituting equation (19) into equation (11) and equating all the coefficients of x, y, z, t, and their multiples equal to zero. Then, a system of algebraic equations consisting of l_r, m_r, n_r, w_r, δ_1, δ_2, and η with $1 \le r \le 3$ is obtained. By solving the system of equations using symbolic software Maple, we obtain the values of some parameters:

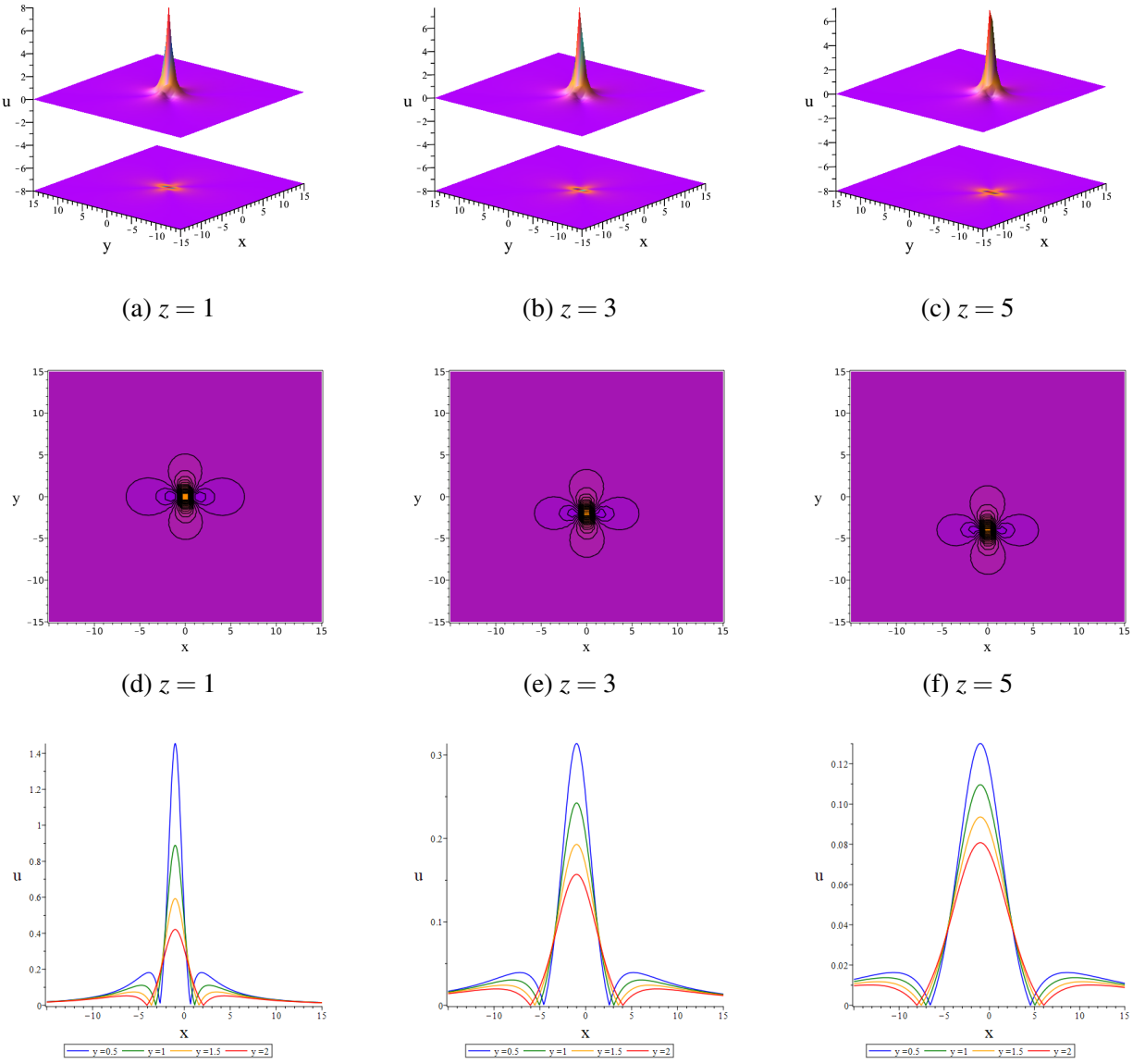

(a) $z = 1$ (b) $z = 3$ (c) $z = 5$

(d) $z = 1$ (e) $z = 3$ (f) $z = 5$

(g) $z = 1$ (h) $z = 3$ (i) $z = 5$

Fig. 2 Wave profiles of the lump wave solution for equation (18) with different values of z: **(a)-(c)** are the 3D profiles with density plots; **(d)-(f)** are the contour plots; and **(g)-(i)** are the wave propagation along the x-axis.

Case I.

$$l_1 = 0, l_2 = -\frac{-\kappa_2 n_2 \kappa_5 + \kappa_6 n_2 \kappa_3 + w_2 \kappa_1 \kappa_3}{\kappa_3 \kappa_4}, m_1 = -\frac{\kappa_2 n_1}{\kappa_3}, m_2 = -\frac{\kappa_2 n_2}{\kappa_3},$$
$$m_3 = -\frac{\kappa_2 n_3}{\kappa_3}, w_1 = \frac{n_1 (\kappa_2 \kappa_5 - \kappa_3 \kappa_6)}{\kappa_3 \kappa_1}, w_3 = \frac{-l_3 \kappa_4 \kappa_3 + \kappa_2 \kappa_5 n_3 - \kappa_3 n_3 \kappa_6}{\kappa_3 \kappa_1}. \tag{20}$$

Substituting the parameter values of equation (20) into equation (19), we attain

$$f=\left(-\frac{\kappa_2 n_1 y}{\kappa_3}+n_1 z+\frac{t n_1\left(\kappa_2\kappa_5-\kappa_3\kappa_6\right)}{\kappa_3\kappa_1}+\delta_1\right)^2+\left(-\frac{\left(-\kappa_2 n_2\kappa_5+\kappa_6 n_2\kappa_3+w_2\kappa_1\kappa_3\right)x}{\kappa_3\kappa_4}-\frac{\kappa_2 n_2 y}{\kappa_3}+n_2 z+w_2 t+\delta_2\right)^2+ \mathrm{e}^{l_3 x-\frac{\kappa_2 n_3 y}{\kappa_3}+n_3 z+\frac{t\left(-l_3\kappa_4\kappa_3+\kappa_2\kappa_5 n_3-\kappa_3 n_3\kappa_6\right)}{\kappa_3\kappa_1}}+\eta. \tag{21}$$

Substituting the expression (21) into equation (6) yields the appropriate solutions to the KDKK and BK equations (1), which reveals the collisions of the single-lump and solitary-wave solutions. Taking the specific value of the free parameters: $l_3=1$, $n_1=n_2=n_3=1$, $w_2=1$, $\delta_1=\delta_2=1$, $\kappa_1=1$, $\kappa_2=1$, $\kappa_3=1$, $\kappa_4=-2$, $\kappa_5=\kappa_6=1$, and $\eta=1$. The specific wave solution of the governing equation (1) is

$$u=\frac{1+2e^{\phi_1}}{e^{\phi_1}+t^2+(x-2y+2z+2)t+\frac{x^2}{4}+(1-y+z)x+2y^2-4(z+1)y+2z^2+4z+3}-\frac{\frac{1}{2}\left(x-2y+2z+2t+2+2e^{\phi_1}\right)^2}{\left(e^{\phi_1}+t^2+(x-2y+2z+2)t+\frac{x^2}{4}+(1-y+z)x+2y^2-4(z+1)y+2z^2+4z+3\right)^2}, \tag{22}$$

where $\phi_1=x-y+z+2t$. Its propagation velocity along the xy-plane is shown in Fig. 3.

Case II.

$$m_1=-\frac{\kappa_2 n_1}{\kappa_3}, m_2=-\frac{\kappa_2 n_2}{\kappa_3}, m_3=-\frac{\kappa_2 n_3}{\kappa_3}, w_1=\frac{\kappa_2\kappa_5 n_1-\kappa_3 l_1\kappa_4-\kappa_3 n_1\kappa_6}{\kappa_3\kappa_1}, \\ w_2=\frac{\kappa_2 n_2\kappa_5-l_2\kappa_3\kappa_4-\kappa_6 n_2\kappa_3}{\kappa_3\kappa_1}, w_3=\frac{\kappa_2\kappa_5 n_3-l_3\kappa_4\kappa_3-\kappa_3 n_3\kappa_6}{\kappa_3\kappa_1}. \tag{23}$$

Substituting the parameter values of equation (23) into equation (19), we attain

$$f=\left(l_1 x-\frac{\kappa_2 n_1 y}{\kappa_3}+n_1 z+\frac{t\left(-\kappa_3 l_1\kappa_4+\kappa_2\kappa_5 n_1-\kappa_3 n_1\kappa_6\right)}{\kappa_3\kappa_1}+\delta_1\right)^2+\left(l_2 x-\frac{\kappa_2 n_2 y}{\kappa_3}+n_2 z+\frac{t\left(-l_2\kappa_3\kappa_4+\kappa_2 n_2\kappa_5-\kappa_6 n_2\kappa_3\right)}{\kappa_3\kappa_1}+\delta_2\right)^2+ \mathrm{e}^{l_3 x-\frac{\kappa_2 n_3 y}{\kappa_3}+n_3 z+\frac{t\left(-l_3\kappa_4\kappa_3+\kappa_2\kappa_5 n_3-\kappa_3 n_3\kappa_6\right)}{\kappa_3\kappa_1}}+\eta. \tag{24}$$

Substituting the expression (24) into equation (6) yields the appropriate solutions to the KDKK and BK equations (1), which reveals the collision of the single-lump and solitary-wave. Taking the specific value of the free parameters: $l_1=l_3=1$, $l_2=-1$, $n_1=-3$, $n_2=n_3=1$, $\delta_1=\delta_2=1$, $\kappa_1=1$, $\kappa_2=1$, $\kappa_3=1$, $\kappa_4=-1$, $\kappa_5=-1$, $\kappa_6=1$, and $\eta=1$. The specific wave solution of the governing equation (1) is

$$u=\frac{4+2e^{\phi_2}}{e^{\phi_2}+45t^2+6(x+7y-7z+1)t+x^2+2(y-z-1)x+10y^2+4(1-5z)y+10z^2-4z+3}-\frac{2\left(2x+2y-2z+6t-2+e^{\phi_2}\right)^2}{\left(e^{\phi_2}+45t^2+6(x+7y-7z+1)t+x^2+2(y-z-1)x+10y^2+4(1-5z)y+10z^2-4z+3\right)^2}, \tag{25}$$

where $\phi_2=x-y+z-t$. Its propagation velocity along the xy-plane is shown in Fig. 4.

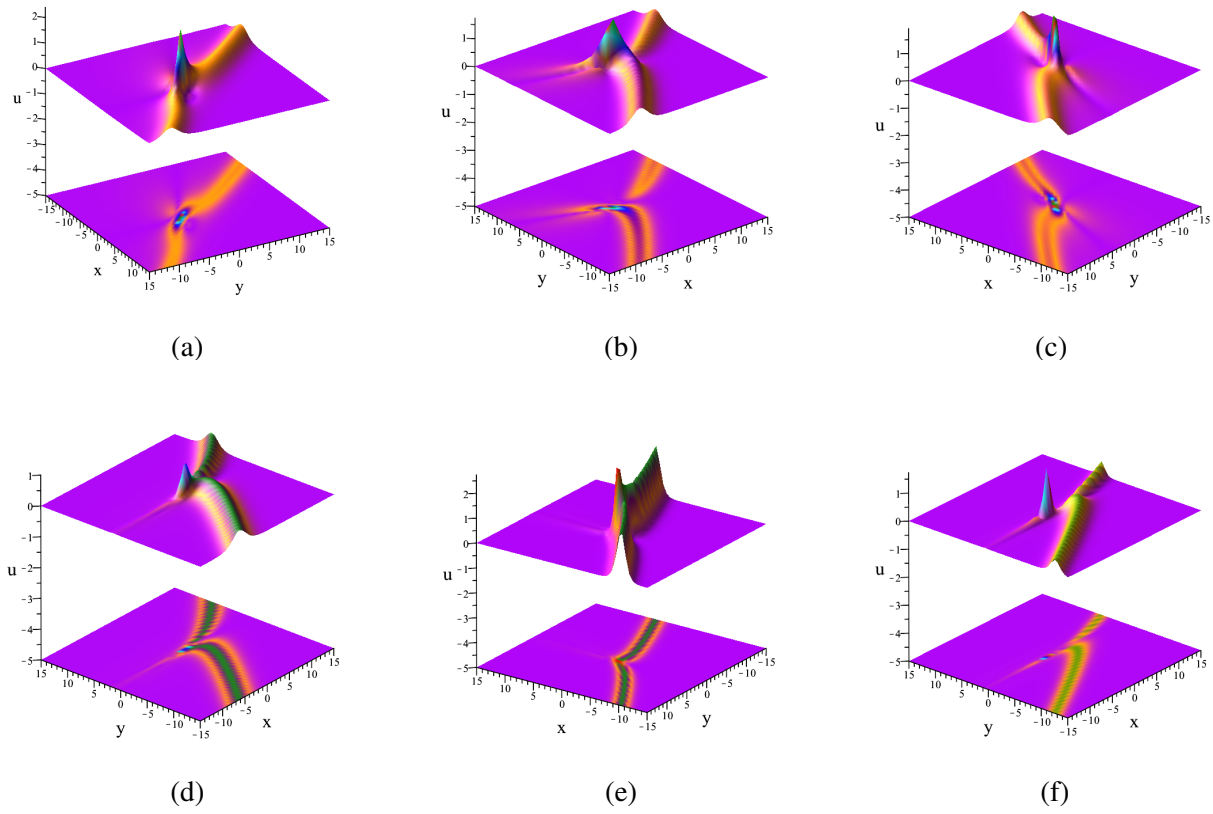

Fig. 3 The 3D profiles with density plots show the collisions of the single-lump and solitary-wave solutions to equation (22) using different parameters.

4.3 Collision of waves: lump wave and periodic wave

Assume a function that combines the sine and quadratic functions to examine the conflict of the lump and periodic wave solutions of the KDKK and BK equations (1). For example,

$$f = (l_1x+m_1y+n_1z+w_1t+\delta_1)^2+(l_2x+m_2y+n_2z+w_2t+\delta_2)^2+sin(l_3x+m_3y+n_3z+w_3t)+\eta, \quad (26)$$

where l_r, m_r, n_r, w_r, δ_1, δ_2, and η are free parameters with $r = 1,2,3$ to be determined. Substituting equation (26) into equation (11) and applying the same procedure as before. A system of algebraic equations involving l_r, m_r, n_r, w_r, δ_1, δ_2, and η is obtained, where $1 \leq r \leq 3$. Solving the system of equations using the symbolic software Maple, we obtain the values of some parameters:

Case I.

$$l_1 = 0, l_2 = -\frac{w_2\kappa_1+m_2\kappa_5+n_2\kappa_6}{\kappa_4}, l_3 = 0, m_1 = 0, n_1 = 0, n_2 = -\frac{\kappa_3 m_2}{\kappa_2}, w_1 = 0, w_3 = -\frac{m_3\kappa_5+n_3\kappa_6}{\kappa_1}. \quad (27)$$

Substituting the parameter values of equation (27) into equation (26), we attain

$$f = \delta_1^2+\left(-\frac{\left(m_2\kappa_5-\frac{\kappa_3 m_2\kappa_6}{\kappa_2}+w_2\kappa_1\right)x}{\kappa_4}+m_2y-\frac{\kappa_3 m_2 z}{\kappa_2}+w_2t+\delta_2\right)^2- \sin\left(-m_3y-n_3z+\frac{t\left(m_3\kappa_5+n_3\kappa_6\right)}{\kappa_1}\right)+\eta. \quad (28)$$

Substituting the expression (28) into equation (6) yields the appropriate solution to equation (1), which reveals the conflict between the lump wave and periodic wave. Choosing the particular value of the free parameters: $m_2 = m_3 = n_3 = w_2 = 1$, $\delta_1 = \delta_2 = 1$, $\kappa_1 = 1$, $\kappa_2 = -1$, $\kappa_3 = 1$, $\kappa_4 = -3$, $\kappa_5 = \kappa_6 = 1$, and $\eta = 1$. The particular wave solution of the KDKK and BK equations (1) is

$$u = -\frac{\sin(2t - F_1 + 1) + t^2 + 2(x + F_1)t + x^2 + 2F_1 x + y^2 + 2(1+z)y + z^2 + 2z - 1}{\left(-\frac{1}{2}\sin(2t - F_1 + 1) + \frac{1}{2}(x^2 + y^2 + z^2 + t^2 + 3) + (x + F_1)t + F_1 x + (1+z)y + z\right)^2}, \tag{29}$$

where $F_1 = 1 + y + z$. Its propagation velocity along the xy-plane, xz-plane, and xt-plane are shown in Fig. 5.

Case II.

$$\begin{aligned} &l_1 = 0, l_2 = -\frac{m_1 w_2 \kappa_5 - m_2 w_1 \kappa_5 + n_1 \kappa_6 w_2 - n_2 \kappa_6 w_1}{\kappa_4 w_1}, l_3 = 0, \\ &n_2 = -\frac{m_2 \kappa_3}{\kappa_2}, w_1 = -\frac{m_1 \kappa_5 + n_1 \kappa_6}{\kappa_1}, w_3 = \frac{(m_3 \kappa_5 + n_3 \kappa_6) w_1}{m_1 \kappa_5 + n_1 \kappa_6}. \end{aligned} \tag{30}$$

Substituting the parameter values of equation (30) into equation (26), we attain

$$\begin{aligned} f = &\left(m_1 y + n_1 z - \frac{t(m_1 \kappa_5 + n_1 \kappa_6)}{\kappa_1} + \delta_1\right)^2 + \left(m_2 y - \frac{\kappa_3 m_2 z}{\kappa_2} + w_2 t + \delta_2 + \right. \\ &\left. \frac{\left(m_1 w_2 \kappa_5 + \frac{m_2 (m_1 \kappa_5 + n_1 \kappa_6)\kappa_5}{\kappa_1} + n_1 \kappa_6 w_2 - \frac{\kappa_3 m_2 (m_1 \kappa_5 + n_1 \kappa_6)\kappa_6}{\kappa_2 \kappa_1}\right) \kappa_1 x}{\kappa_4 (m_1 \kappa_5 + n_1 \kappa_6)}\right)^2 - \\ &\sin\left(-m_3 y - n_3 z + \frac{t(m_3 \kappa_5 + n_3 \kappa_6)}{\kappa_1}\right) + \eta. \end{aligned} \tag{31}$$

Substituting the expression (31) into equation (6) yields the appropriate solution to equation (1), which reveals the collision of periodic and lump wave. Choosing the particular value of the free parameters: $\kappa_1 = 1$, $\kappa_2 = 1$, $\kappa_3 = 1$, $\kappa_4 = -1$, $\kappa_5 = 1$, $\kappa_6 = 1$, $m_1 = i$, $m_2 = m_3 = 1$, $n_1 = n_3 = 1$, $w_2 = 1$, $\delta_1 = \delta_2 = 1$, and $\eta = -\frac{1}{2}$. The particular wave solution of the KDKK and BK equations (1) is

$$\begin{aligned} u = &\frac{8}{2\left(1 + iy + z - (1+i)t\right)^2 + 2(1 - x + y - z + t)^2 - 2\sin(2t - y - z) - 1} - \\ &\frac{8(1 - x + y - z + t)^2}{\left(\left(1 + iy + z - (1+i)t\right)^2 + (1 - x + y - z + t)^2 - \frac{1}{2} - \sin(2t - y - z)\right)^2}. \end{aligned} \tag{32}$$

The interaction of the periodic and lump wave solutions of equation (32) over time is shown in Fig. 6 through contour plots, 2D profiles, and 3D profiles.

Case III.

$$\begin{aligned} &l_1 = 0, l_2 = -\frac{\kappa_1 m_1 w_2 + n_2 \kappa_6 m_1 - n_1 m_2 \kappa_6}{\kappa_4 m_1}, l_3 = 0, m_1 = -\frac{n_1 \kappa_6}{\kappa_5}, \\ &n_2 = -\frac{\kappa_3 m_2}{\kappa_2}, w_1 = 0, w_3 = -\frac{\kappa_6 (m_1 n_3 - m_3 n_1)}{\kappa_1 m_1}. \end{aligned} \tag{33}$$

Substituting the parameter values of equation (33) into equation (26), we attain

$$\begin{aligned} f = &\left(-\frac{n_1 \kappa_6 y}{\kappa_5} + n_1 z + \delta_1\right)^2 + \left(\frac{\left(-\frac{\kappa_1 n_1 \kappa_6 w_2}{\kappa_5} + \frac{n_1 \kappa_6^2 \kappa_3 m_2}{\kappa_5 \kappa_2} - n_1 m_2 \kappa_6\right) \kappa_5 x}{\kappa_4 n_1 \kappa_6} + m_2 y - \frac{\kappa_3 m_2 z}{\kappa_2} + w_2 t + \delta_2\right)^2 + \\ &\sin\left(m_3 y + n_3 z + \frac{t\left(-\frac{n_1 \kappa_6 n_3}{\kappa_5} - m_3 n_1\right) \kappa_5}{\kappa_1 n_1}\right) + \eta. \end{aligned} \tag{34}$$

Substituting the expression (34) into equation (6) yields the appropriate solutions to equation (1), which reveals the collision between periodic and lump wave. Choosing the particular value of the free parameters $m_2 = m_3 = 1$, $n_1 = i, n_3 = -1, w_2 = 1, \delta_1 = \delta_2 = 1, \kappa_1 = 1, \kappa_2 = 1, \kappa_3 = 1, \kappa_4 = -2, \kappa_5 = -1, \kappa_6 = 1$, and $\eta = 1$. The particular wave solution of the KDKK and BK equations (1) is

$$u = \frac{1}{(1+iy+iz)^2 + F_2^2 + \sin(2t+y-z)+1} - \frac{2F_2^2}{\left((1+iy+iz)^2 + F_2^2 + \sin(2t+y-z)+1\right)^2}, \tag{35}$$

where $F_2 = 1 - \frac{x}{2} + y - z + t$. Its propagation velocity is shown in Fig. 7.

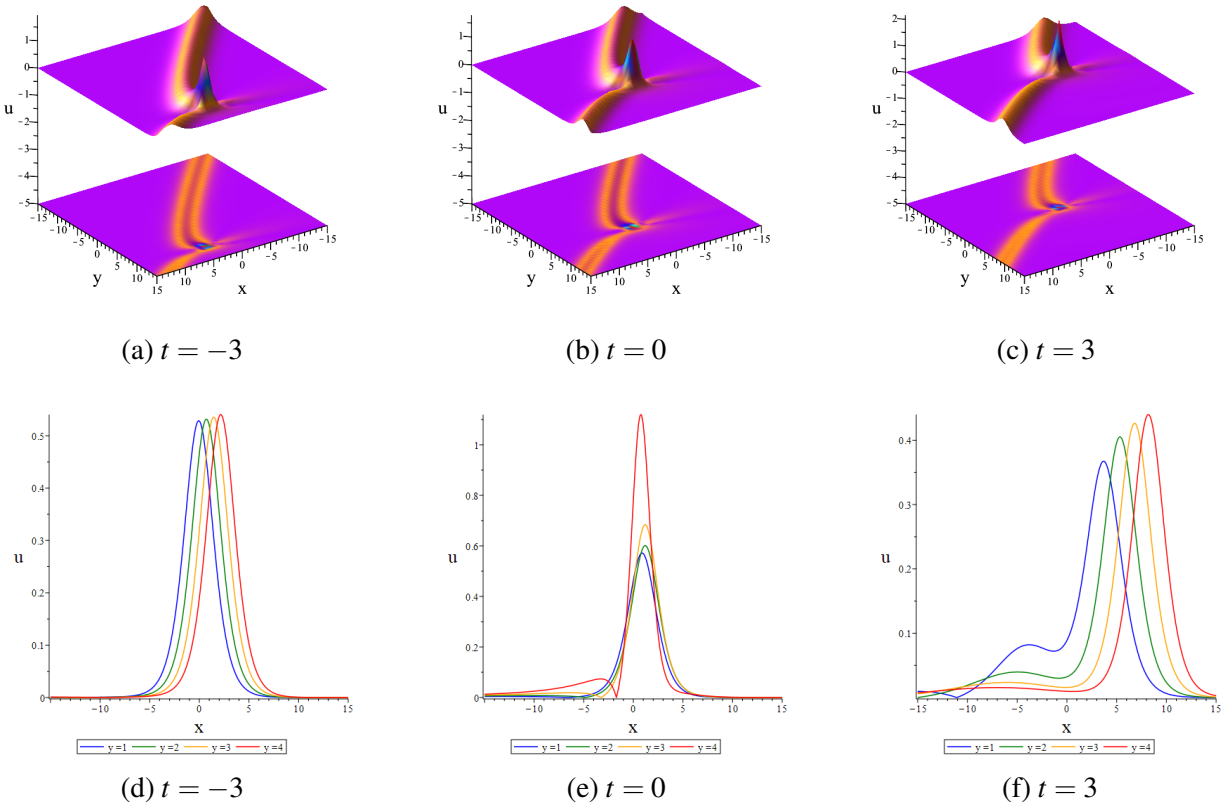

(a) $t = -3$ (b) $t = 0$ (c) $t = 3$

(d) $t = -3$ (e) $t = 0$ (f) $t = 3$

Fig. 4 Collisions of single-lump and solitary-wave solutions of equation (25): **(a)-(c)** are the 3D profiles with density plots; and **(d)-(f)** are the corresponding 2D wave propagation along the x-axis.

4.4 Collision of waves: solitary, periodic, and lump waves

Consider a function that combines exponential, quadratic, and cosine functions to analyze the conflict that arises between solitary, periodic, and lump wave solutions of the KDKK and BK equation (1), that is,

$$\begin{aligned} f =& (l_1x + m_1y + n_1z + w_1t + \delta_1)^2 + (l_2x + m_2y + n_2z + w_2t + \delta_2)^2 + cos(l_3x + m_3y + n_3z + w_3t) + \\ & exp(l_3x + m_3y + n_3z + w_3t) + \eta, \end{aligned} \tag{36}$$

where l_r, m_r, n_r, w_r, δ_1, δ_2, and η are free parameters with $r = 1, 2, 3$ to be determined. Substituting equation (36) into equation (11) and following the same procedure as before. A system of algebraic equations consisting

of l_r, m_r, n_r, w_r, δ_1, δ_2, and η with $1 \leq r \leq 3$ is obtained. Solving the system of equations using the symbolic software Maple, we obtain the values of some parameters:

Case I.

$$\begin{aligned} &l_1 = 0, l_2 = -\frac{\kappa_1\kappa_2 n_2 w_1 + w_2\kappa_1\kappa_3 m_1 + \kappa_2 n_1 n_2\kappa_6 + n_2\kappa_6\kappa_3 m_1}{\kappa_4\kappa_3 m_1}, l_3 = 0, l_4 = 0, \\ &m_1 = -\frac{w_1\kappa_1 + n_1\kappa_6}{\kappa_5}, m_2 = -\frac{\kappa_2 n_2}{\kappa_3}, n_3 = -\frac{w_3\kappa_1 m_1 - \kappa_1 m_3 w_1 - m_3 n_1\kappa_6}{m_1\kappa_6}, \\ &n_4 = -\frac{w_4\kappa_1 m_1 - \kappa_1 m_4 w_1 - m_4 n_1\kappa_6}{m_1\kappa_6}. \end{aligned} \tag{37}$$

Substituting the parameter values of equation (37) into equation (36), we attain

$$\begin{aligned} f = &\left(-\frac{(\kappa_1 w_1 + n_1\kappa_6)y}{\kappa_5} + n_1 z + w_1 t + \delta_1\right)^2 + \left(-\frac{\kappa_2 n_2 y}{\kappa_3} + n_2 z + w_2 t + \delta_2 + \right. \\ &\left.\frac{\left(\kappa_1\kappa_2 n_2 w_1 - \frac{\kappa_1\kappa_3(\kappa_1 w_1 + n_1\kappa_6)w_2}{\kappa_5} + \kappa_2 n_1 n_2\kappa_6 - \frac{\kappa_3(\kappa_1 w_1 + n_1\kappa_6)n_2\kappa_6}{\kappa_5}\right)\kappa_5 x}{\kappa_4\kappa_3(\kappa_1 w_1 + n_1\kappa_6)}\right)^2 + \\ &\cos\left(-m_3 y - \frac{\left(-\frac{\kappa_1(\kappa_1 w_1 + n_1\kappa_6)w_3}{\kappa_5} - \kappa_1 m_3 w_1 - m_3 n_1\kappa_6\right)\kappa_5 z}{(\kappa_1 w_1 + n_1\kappa_6)\kappa_6} - w_3 t\right) + \\ &e^{m_4 y + \frac{\left(-\frac{\kappa_1(\kappa_1 w_1 + n_1\kappa_6)w_4}{\kappa_5} - \kappa_1 m_4 w_1 - m_4 n_1\kappa_6\right)\kappa_5 z}{(\kappa_1 w_1 + n_1\kappa_6)\kappa_6} + w_4 t} + \eta. \end{aligned} \tag{38}$$

Substituting the expression (38) into equation (6) yields the appropriate solutions to the KDKK and BK equations (1), which reveals the collision of solitary, periodic, and lump waves. Taking the specific value of the parameters: $m_3 = -0.2$, $m_4 = 0.4$, $n_1 = 0.3$, $n_2 = -i$, $w_1 = 0.1$, $w_2 = 0.1$, $w_3 = 0.2$, $w_4 = 0.5$, $\delta_1 = \delta_2 = 1.5$, $\kappa_1 = 1$, $\kappa_2 = 0.5$, $\kappa_3 = 1$, $\kappa_4 = -4.5$, $\kappa_5 = -1$, $\kappa_6 = 1$, and $\eta = -0.6$. The specific wave solution of the governing equation (1) is

$$\begin{aligned} u = &-\frac{0.4 + 0.06i}{(0.4y + 0.3z + 0.1t + 1.5)^2 + P^2 - 0.6 + \cos(-0.2y - 0.4z + 0.2t) + e^{0.4y - 0.1z + 0.5t}} + \\ &\frac{(0.9 + 0.12i)((0.02 - 0.3i)x + 0.5iy - iz + 0.1t + 1.5)^2}{\left((0.4y + 0.3z + 0.1t + 1.5)^2 + P^2 - 0.6 + \cos(-0.2y - 0.4z + 0.2t) + e^{0.4y - 0.1z + 0.5t}\right)^2}, \end{aligned} \tag{39}$$

where $P = (0.02 - 0.3i)x + 0.5iy - iz + 0.1t + 1.5$. Fig. 8 illustrates the interaction of solitary, periodic, and lump wave solutions of equation (39) through contour plots, 2D profiles, and 3D profiles.

Case II.

$$\begin{aligned} &l_1 = l_3 = l_4 = 0, l_2 = -\frac{w_2\kappa_1}{\kappa_4}, m_1 = m_2 = 0, n_1 = -\frac{w_1\kappa_1}{\kappa_6}, \\ &n_2 = 0, n_3 = -\frac{w_3\kappa_1 + m_3\kappa_5}{\kappa_6}, n_4 = -\frac{w_4\kappa_1 + m_4\kappa_5}{\kappa_6}. \end{aligned} \tag{40}$$

Substituting the parameter values of equation (40) into equation (36), we attain

$$\begin{aligned} f = &\left(-\frac{w_1\kappa_1 z}{\kappa_6} + w_1 t + \delta_1\right)^2 + \left(-\frac{w_2\kappa_1 x}{\kappa_4} + w_2 t + \delta_2\right)^2 - \\ &\sin\left(-m_3 y + \frac{(w_3\kappa_1 + m_3\kappa_5)z}{\kappa_6} - w_3 t\right) + e^{m_4 y - \frac{(w_4\kappa_1 + m_4\kappa_5)z}{\kappa_6} + w_4 t} + \eta. \end{aligned} \tag{41}$$

Substituting the expression (41) into equation (6) yields the appropriate solutions to the KDKK and BK equations (1), which reveals the collision of solitary, periodic, and lump waves. Taking the specific value of the free

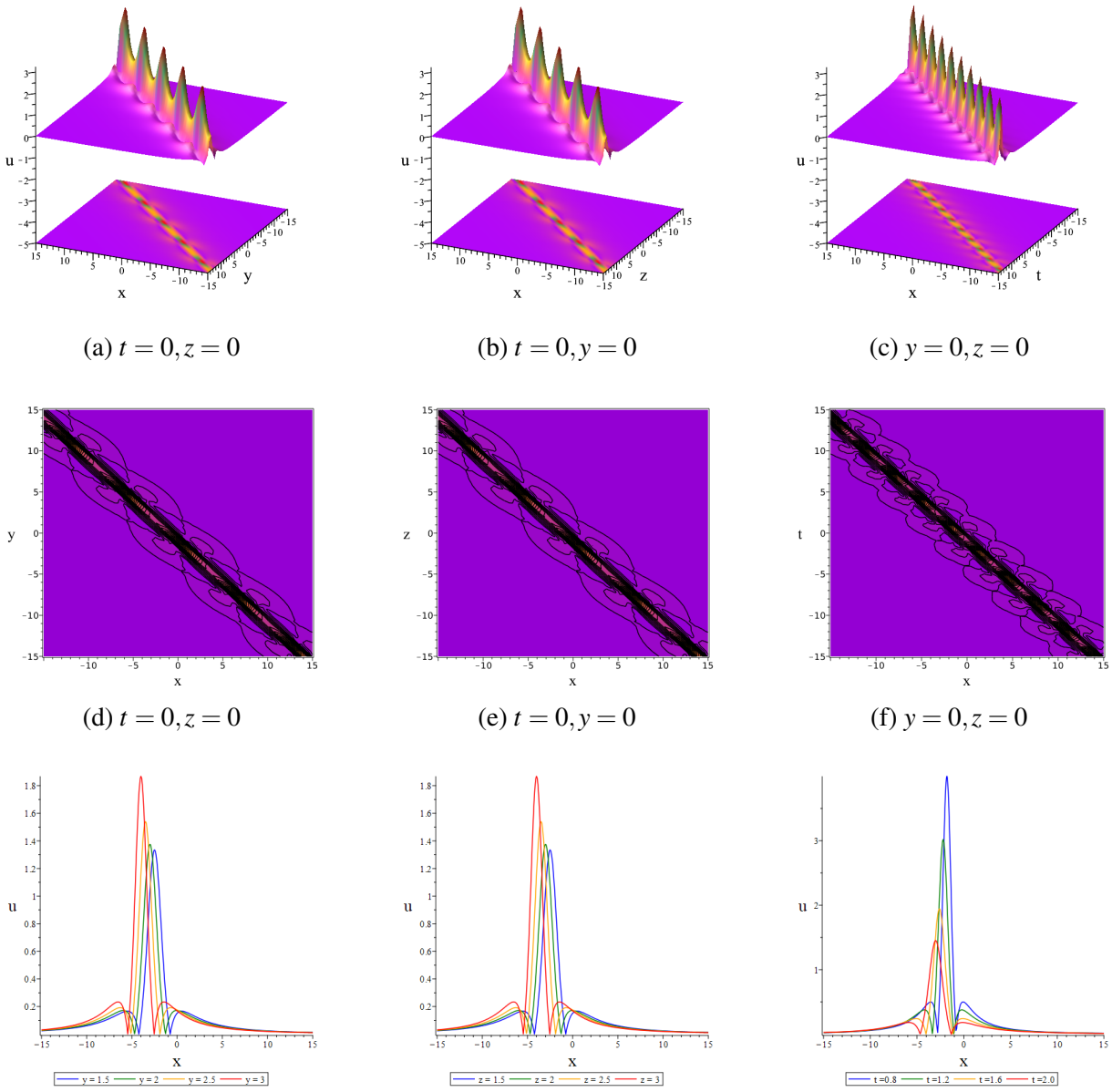

(a) $t=0,z=0$ (b) $t=0,y=0$ (c) $y=0,z=0$

(d) $t=0,z=0$ (e) $t=0,y=0$ (f) $y=0,z=0$

(g) $t=0,z=0$ (h) $t=0,y=0$ (i) $y=0,z=0$

Fig. 5 Collision of periodic and lump wave solutions of equation (29): **(a)-(c)** display 3D profiles with density plots; **(d)-(f)** display contour plots; and **(g)-(i)** display 2D wave profiles.

parameters: $m_3=-1$, $m_4=0.5$, $w_1=0.8$, $w_2=0.1$, $w_3=0.6$, $w_4=0.3$, $\delta_1=\delta_2=1.5$, $\eta=-0.3$, $\kappa_1=2$, $\kappa_2=0.2$, $\kappa_3=1$, $\kappa_4=-2$, $\kappa_5=-1$, and $\kappa_6=1$. The specific wave solution of the governing equation (1) is

$$u=\frac{0.04}{(-1.6z+0.8t+1.5)^2+(0.1x+0.1t+1.5)^2-0.3+\sin(-y-2.2z+0.6t)+e^{0.5y-0.1z+0.3t}}-\frac{0.08\,(0.1x+0.1t+1.5)^2}{\left((-1.6z+0.8t+1.5)^2+(0.1x+0.1t+1.5)^2-0.3+\sin(-y-2.2z+0.6t)+e^{0.5y-0.1z+0.3t}\right)^2}. \tag{42}$$

Its propagation velocity along the xy-plane is shown in Fig. 9.

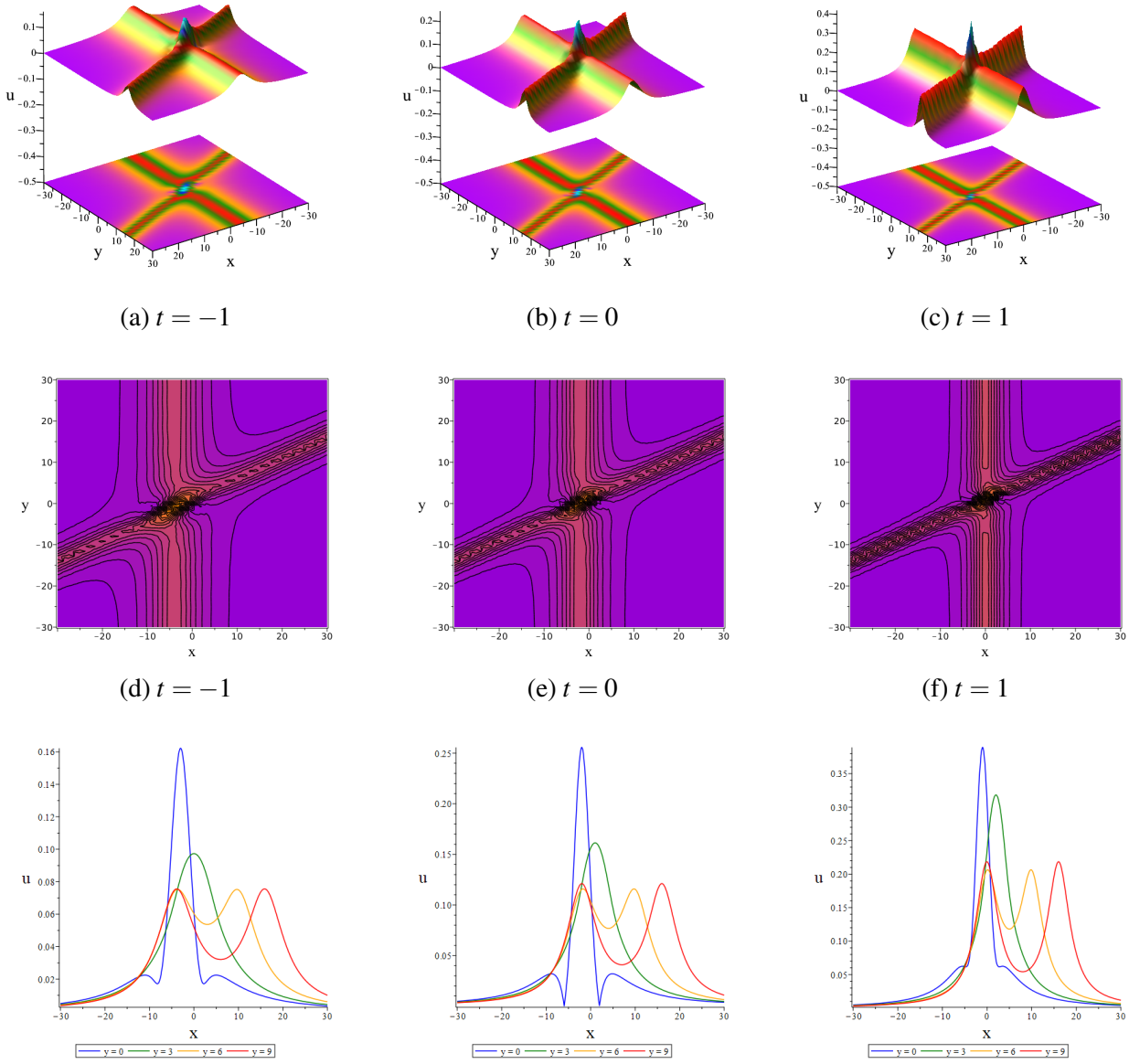

(a) $t=-1$ (b) $t=0$ (c) $t=1$

(d) $t=-1$ (e) $t=0$ (f) $t=1$

(g) $t=-1$ (h) $t=0$ (i) $t=1$

Fig. 6 Collision of periodic and lump wave solutions of equation (32): **(a)-(c)** are the 3D profiles with density plots; **(d)-(f)** are the contour plots; and **(g)-(i)** are the corresponding 2D wave propagation, respectively.

4.5 Collision of waves: lump and breather waves

Consider a function that combines cosine, the double exponential, and quadratic functions to test the collision of lump and breather wave solutions of KDKK and BK equations (1), that is,

$$\begin{aligned} f =&(l_1x+m_1y+n_1z+w_1t+\delta_1)^2+(l_2x+m_2y+n_2z+w_2t+\delta_2)^2+cos(l_3x+m_3y+n_3z+w_3t+\delta_3)+\\ &exp(l_4x+m_4y+n_4z+w_4t+\delta_4)+exp(-l_4x-m_4y-n_4z-w_4t-\delta_4)+\eta, \end{aligned} \tag{43}$$

where l_r, m_r, n_r, w_r, δ_r, and η are free parameters with $r=1,2,3,4$ to be determined. Substituting equation (43) into equation (11) and following the same procedure as before. Then, a system of algebraic equations involving

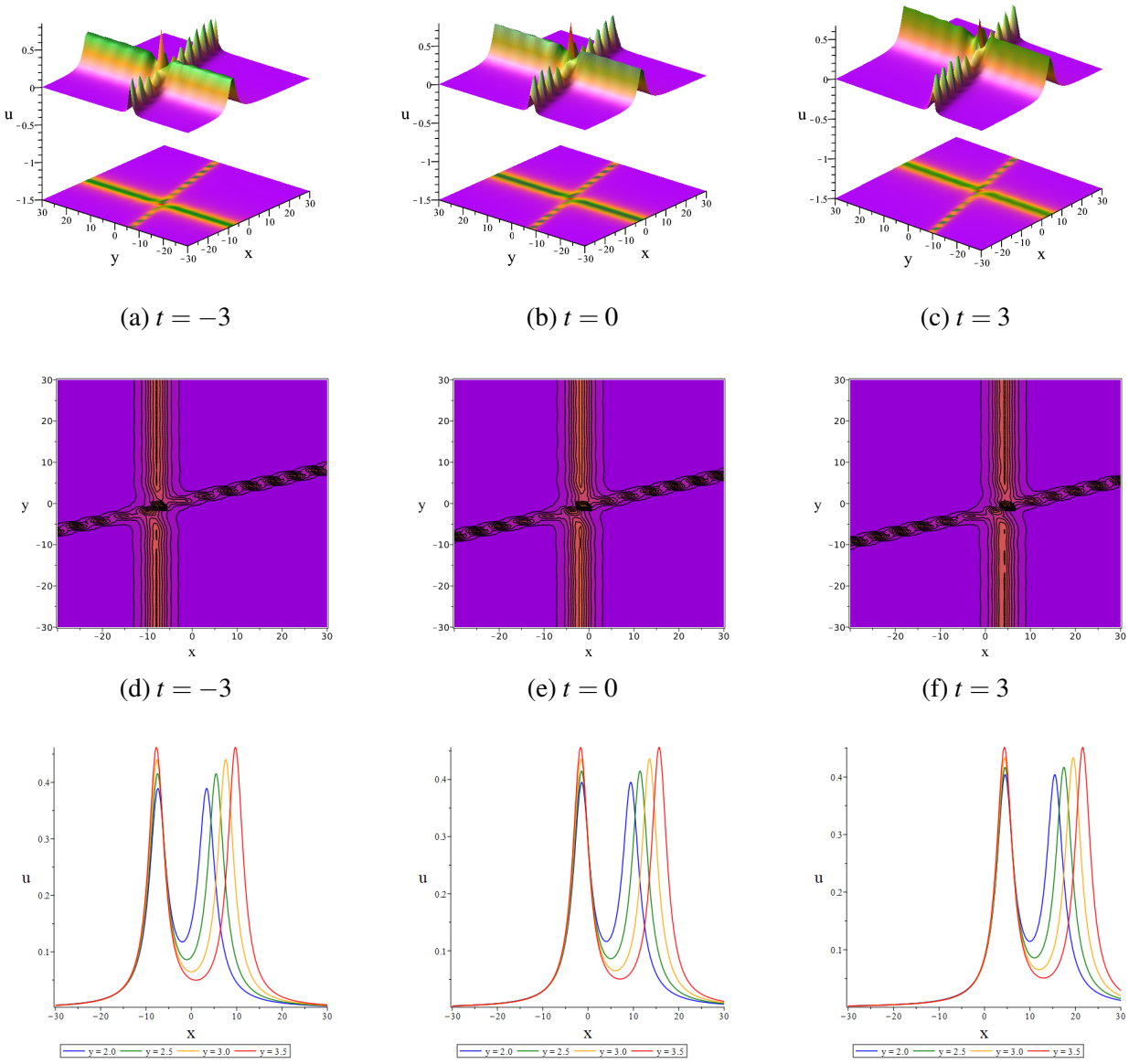

(a) $t = -3$ (b) $t = 0$ (c) $t = 3$

(d) $t = -3$ (e) $t = 0$ (f) $t = 3$

(g) $t = -3$ (h) $t = 0$ (i) $t = 3$

Fig. 7 Collision of periodic and lump wave solutions of equation (35): 3D profiles with density plots are shown in **(a)-(c)**; contour plots are shown in **(d)-(f)**; and 2D wave propagation along the x-axis is shown in **(g)-(i)**.

l_r, m_r, n_r, w_r, δ_r, and η is obtained, where $1 \leq r \leq 4$. Solving the system of equations using the symbolic software Maple, we obtain the values of some parameters:

$$
\begin{aligned}
&l_1 = 0, l_2 = -\frac{\kappa_1\kappa_2 n_2 w_1 + w_2\kappa_1\kappa_3 m_1 + \kappa_2 n_1 n_2\kappa_6 + n_2\kappa_6\kappa_3 m_1}{\kappa_4\kappa_3 m_1}, l_3 = 0, l_4 = 0,\\
&m_1 = -\frac{w_1\kappa_1 + n_1\kappa_6}{\kappa_5}, m_2 = -\frac{\kappa_2 n_2}{\kappa_3}, n_3 = -\frac{w_3\kappa_1 m_1 - \kappa_1 m_3 w_1 - m_3 n_1\kappa_6}{m_1\kappa_6},\\
&n_4 = -\frac{w_4\kappa_1 m_1 - \kappa_1 m_4 w_1 - m_4 n_1\kappa_6}{m_1\kappa_6}.
\end{aligned}
\tag{44}
$$

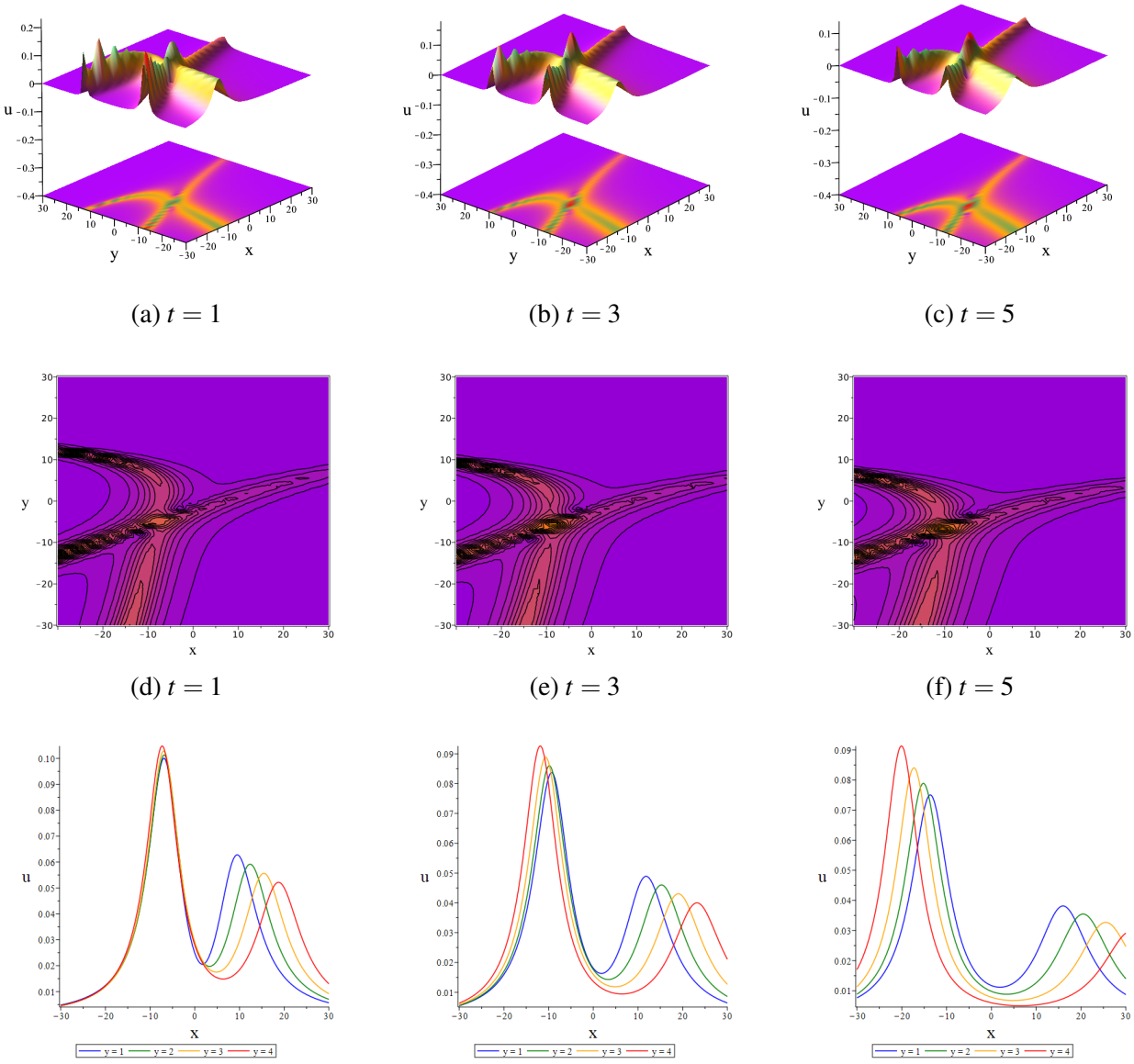

(a) $t = 1$ (b) $t = 3$ (c) $t = 5$

(d) $t = 1$ (e) $t = 3$ (f) $t = 5$

(g) $t = 1$ (h) $t = 3$ (i) $t = 5$

Fig. 8 Collision of solitary, periodic, and lump wave solutions of equation (39): **(a)-(c)** display 3D profiles with density plots; **(d)-(f)** display contour plots; and **(g)-(i)** display 2D wave propagation along the x-axis.

Substituting the parameter values of equation (44) into equation (43), we attain

$$
\begin{aligned}
f = &\left(-\frac{(\kappa_1 w_1 + n_1 \kappa_6)\, y}{\kappa_5} + n_1 z + w_1 t + \delta_1\right)^2 + \Bigg(-\frac{\kappa_2 n_2 y}{\kappa_3} + n_2 z + w_2 t + \delta_2 + \\
&\frac{\left(\kappa_1 \kappa_2 n_2 w_1 - \frac{\kappa_1 \kappa_3 (\kappa_1 w_1 + n_1 \kappa_6) w_2}{\kappa_5} + \kappa_2 n_1 n_2 \kappa_6 - \frac{\kappa_3 (\kappa_1 w_1 + n_1 \kappa_6) n_2 \kappa_6}{\kappa_5}\right) \kappa_5 x}{\kappa_4 \kappa_3 (\kappa_1 w_1 + n_1 \kappa_6)}\Bigg)^2 + \\
&\cos\left(-m_3 y - \frac{\left(-\frac{\kappa_1 (\kappa_1 w_1 + n_1 \kappa_6) w_3}{\kappa_5} - \kappa_1 m_3 w_1 - m_3 n_1 \kappa_6\right) \kappa_5 z}{(\kappa_1 w_1 + n_1 \kappa_6)\, \kappa_6} - w_3 t - \delta_3\right) + \\
&e^{m_4 y + S z + w_4 t + \delta_4} + e^{-m_4 y - S z - w_4 t - \delta_4} + \eta,
\end{aligned}
\tag{45}
$$

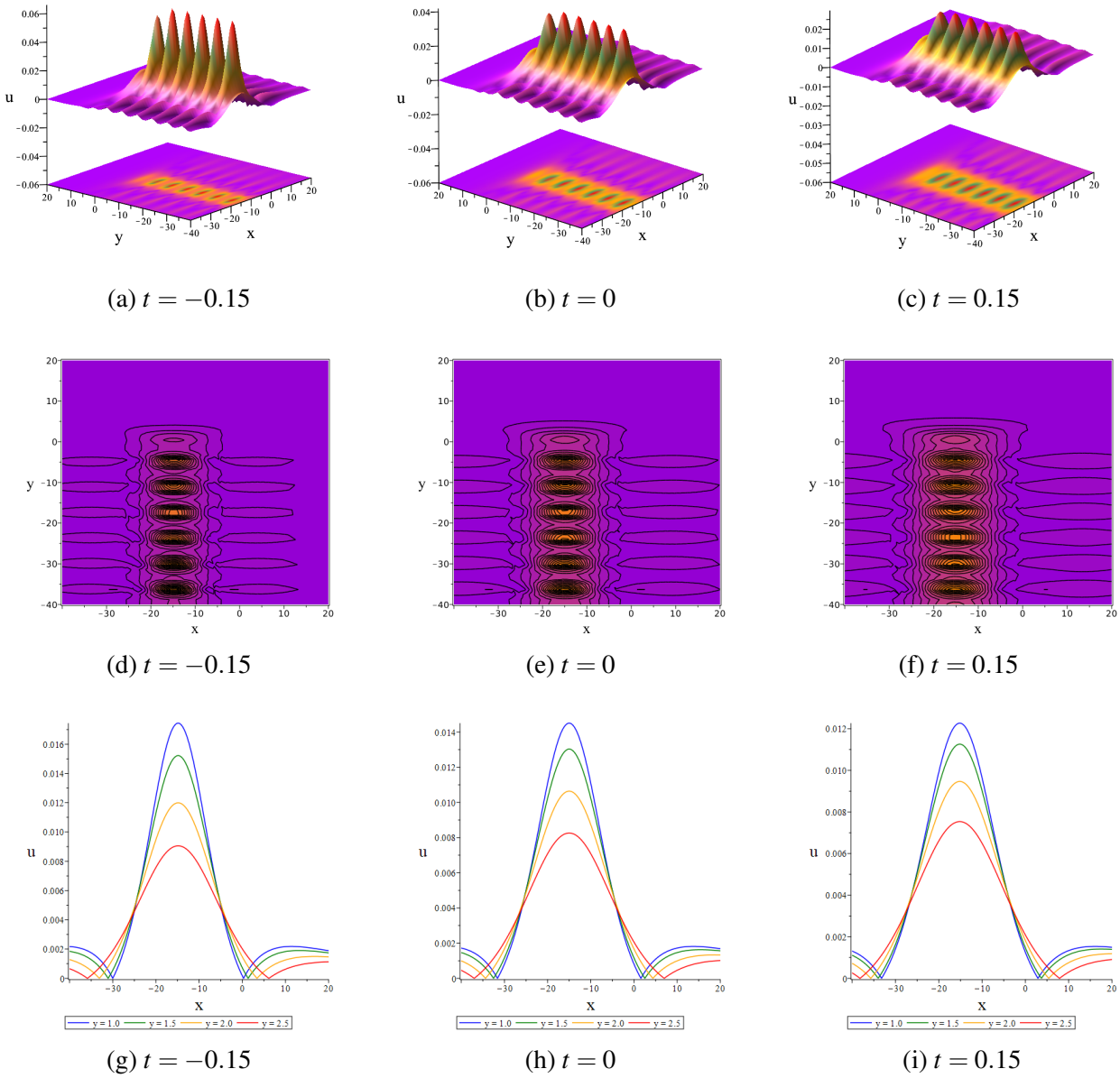

(a) $t = -0.15$ (b) $t = 0$ (c) $t = 0.15$

(d) $t = -0.15$ (e) $t = 0$ (f) $t = 0.15$

(g) $t = -0.15$ (h) $t = 0$ (i) $t = 0.15$

Fig. 9 Collision of solitary, periodic, and lump wave solutions of equation (42): **(a)-(c)** display 3D profiles with density plots; **(d)-(f)** display contour plots; and **(g)-(i)** display 2D wave propagation along the x-axis.

where $S = \dfrac{\left(-\frac{\kappa_1(\kappa_1 w_1 + n_1 \kappa_6)w_4}{\kappa_5} - \kappa_1 m_4 w_1 - m_4 n_1 \kappa_6\right)\kappa_5}{(\kappa_1 w_1 + n_1 \kappa_6)\kappa_6}$.

Substituting the expression (45) into equation (6) yields the appropriate solutions to the KDKK and BK equations (1), which reveals the collision between the breather and lump wave. Choosing the particular value of the free parameters: $m_3 = -0.2$, $m_4 = 0.4$, $n_1 = 0.3$, $n_2 = -i$, $w_1 = 0.1$, $w_2 = 0.2$, $w_3 = 0.3$, $w_4 = 0.4$, $\delta_1 = \delta_2 = \delta_3 = \delta_4 = 1.5$, $\eta = -0.6$, $\kappa_1 = 0.2$, $\kappa_2 = 0.4$, $\kappa_3 = 0.5$, $\kappa_4 = -3$, $\kappa_5 = -1$, and $\kappa_6 = 1$. The specific wave solution of

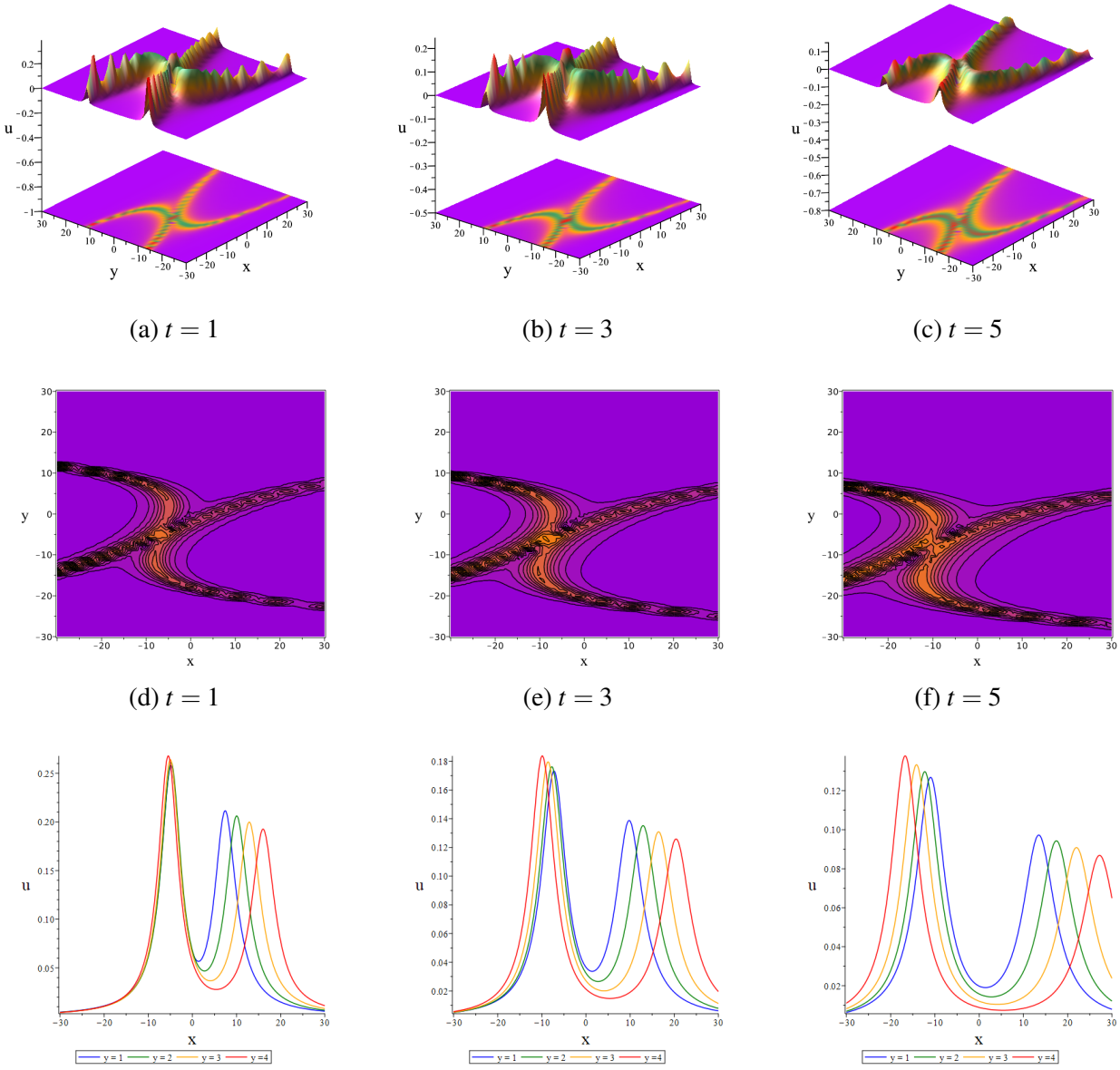

(a) $t = 1$ (b) $t = 3$ (c) $t = 5$

(d) $t = 1$ (e) $t = 3$ (f) $t = 5$

(g) $t = 1$ (h) $t = 3$ (i) $t = 5$

Fig. 10 Collision between lump and breather wave solutions of equation (46): **(a)-(c)** are the 3D profiles with density plots; **(d)-(f)** are the contour plots; and **(g)-(i)** are the corresponding 2D wave propagation, respectively.

the governing equation (1) is

$$u = -\frac{1.4+0.06i}{(0.3y+0.3z+0.1t+1.5)^2+Q^2-0.6+\cos(-0.2y-0.26z+0.3t+1.5)+e^{\omega}+e^{-\omega}}+\frac{(2.88+0.13i)\,Q^2}{\left((0.3y+0.3z+0.1t+1.5)^2+Q^2-0.6+\cos(-0.2y-0.26z+0.3t+1.5)+e^{\omega}+e^{-\omega}\right)^2}, \tag{46}$$

where $Q = (0.013-0.6i)\,x+0.8iy-iz+0.2t+1.5$ and $\omega = 0.4y+0.3z+0.4t+1.5$. Its propagation velocity along the xy-plane is shown in Fig. 10. Lump-breather interactions are elastic because each wave component retains its original velocity, amplitude, and shape; only the phase or position changes before and after the

collision. Therefore, no energy transfer, energy dissipation, or change in waveform is observed within the asymptotic limits.

5 Physical interpretation of the findings

This section presents a comprehensive visual representation of the results from the KDKK and BK equations using the free parameters listed in Table 2, with an emphasis on the absolute components. To determine the amplitude and nature of the fluctuations in the solutions, we examine their absolute components to see how they vary along the absolute axis. This also helps us understand the overall stability and robustness of the solutions.

Table 2 Visual analysis of the KDKK and BK equations for the free parameters.

Fig. No.	Free parameters with intervals
Fig. 1	$\kappa_1 = 1,\ \kappa_2 = 1,\ \kappa_3 = 1,\ \kappa_4 = -2,\ \kappa_5 = -1,\ \kappa_6 = -2,\ l_1 = 1,\ m_2 = 1,\ n_2 = 1,\ w_1 = 1,$ $\delta_1 = \delta_2 = 1,\ \eta = 1,\ z = 1$ for $-15 \le x \le 15,\ -15 \le y \le 15$
Fig. 2	$\kappa_1 = 2,\ \kappa_2 = 2,\ \kappa_3 = 1,\ \kappa_4 = -2,\ \kappa_5 = -1,\ \kappa_6 = 1,\ l_1 = l_2 = 1,\ n_1 = 1,\ w_1 = w_2 = 1,$ $\delta_1 = -1,\ \delta_2 = 1,\ \eta = 1,\ t = 0$ for $-15 \le x \le 15,\ -15 \le y \le 15$
Fig. 3	$\kappa_1 = 1,\ \kappa_2 = 1,\ \kappa_3 = 1,\ \kappa_4 = -2,\ \kappa_5 = \kappa_6 = 1,\ l_3 = 1,\ n_1 = n_2 = n_3 = 1,\ w_2 = 1,\ \delta_1 = 1,$ $\delta_2 = 1,\ \eta = 1,\ z = 1,\ t = 0$ for $-15 \le x \le 15,\ -15 \le y \le 15$
Fig. 4	$\kappa_1 = 1,\ \kappa_2 = 1,\ \kappa_3 = 1,\ \kappa_4 = -1,\ \kappa_5 = -1,\ \kappa_6 = 1,\ l_1 = l_3 = 1,\ l_2 = -1,\ n_1 = -3,$ $n_2 = n_3 = 1,\ \delta_1 = \delta_2 = 1,\ \eta = 1,\ z = 5$ for $-15 \le x \le 15,\ -15 \le y \le 15$
Fig. 5	$\kappa_1 = 1,\ \kappa_2 = -1,\ \kappa_3 = 1,\ \kappa_4 = -3,\ \kappa_5 = \kappa_6 = 1,\ m_2 = m_3 = 1,\ n_3 = 1,\ w_2 = 1,\ \delta_1 = \delta_2 = 1,$ $\eta = 1$ for $-15 \le x \le 15,\ -15 \le y \le 15$
Fig. 6	$\kappa_1 = 1,\ \kappa_2 = 1,\ \kappa_3 = 1,\ \kappa_4 = -1,\ \kappa_5 = 1,\ \kappa_6 = 1,\ m_1 = i,\ m_2 = m_3 = 1,\ n_1 = n_3 = 1,$ $w_2 = 1,\ \delta_1 = \delta_2 = 1,\ \eta = -\frac{1}{2},\ z = 3$ for $-30 \le x \le 30,\ -30 \le y \le 30$
Fig. 7	$\kappa_1 = 1,\ \kappa_2 = 1,\ \kappa_3 = 1,\ \kappa_4 = -2,\ \kappa_5 = -1,\ \kappa_6 = 1,\ m_2 = m_3 = 1,\ n_1 = i,\ n_3 = -1,\ w_2 = 1,$ $\delta_1 = \delta_2 = 1,\ \eta = 1,\ z = 1$ for $-30 \le x \le 30,\ -30 \le y \le 30$
Fig. 8	$\kappa_1 = 1,\ \kappa_2 = 0.5,\ \kappa_3 = 1,\ \kappa_4 = -4.5,\ \kappa_5 = -1,\ \kappa_6 = 1,\ m_3 = -0.2,\ m_4 = 0.4,\ n_1 = 0.3,$ $n_2 = -i,\ w_1 = 0.1,\ w_2 = 0.1,\ w_3 = 0.2,\ w_4 = 0.5,\ \delta_1 = \delta_2 = 1.5,\ \eta = -0.6,\ z = 0$ for $-30 \le x \le 30,\ -30 \le y \le 30$
Fig. 9	$\kappa_1 = 2,\ \kappa_2 = 0.2,\ \kappa_3 = 1,\ \kappa_4 = -2,\ \kappa_5 = -1,\ \kappa_6 = 1,\ m_3 = -1,\ m_4 = 0.5,\ w_1 = 0.8,\ w_2 =$ $0.1,\ w_3 = 0.6,\ w_4 = 0.3,\ \delta_1 = \delta_2 = 1.5,\ \eta = -0.3,\ z = 0$ for $-40 \le x \le 20,\ -40 \le y \le 20$
Fig. 10	$\kappa_1 = 0.2,\ \kappa_2 = 0.4,\ \kappa_3 = 0.5,\ \kappa_4 = -3,\ \kappa_5 = -1,\ \kappa_6 = 1,\ m_3 = -0.2,\ m_4 = 0.4,\ n_1 = 0.3,$ $n_2 = -i,\ w_1 = 0.1,\ w_2 = 0.2,\ w_3 = 0.3,\ w_4 = 0.4,\ \delta_1 = \delta_2 = \delta_3 = \delta_4 = 1.5,\ \eta = -0.6,$ $z = 0$ for $-30 \le x \le 30,\ -30 \le y \le 30$

In Fig. 1, we have illustrated the lump wave solution, where it propagates to the left along the x-axis in (a) and to the right in (b) and (c). The three-dimensional graph of the solution to equation (15) shows a peak in absolute value, and a contour plot displays a flower-like pattern that helps to understand the nature of the solution. Fig. 2 illustrates the nature of the lump wave solutions for different values of z in equation (18). The solutions are shifting to the right along the x-axis, shown as a 3D profile with a density plot and a flower-like contour plot. Fig. 3 illustrates the collision of the solitary and one-lump wave solutions of equation (22), where we have generated 3D profiles and density graphs using different parameters. Using time variation, we analyzed the collision of the solitary and one-lump wave solutions of equation (25) and displayed a 3D profile with density plots and 2D wave propagation along the x-axis, as shown in Fig. 4.

Based on different choices of free parameters and range space, Figs. 5, 6, and 7 illustrate the collision between the lump and periodic wave solutions of equations (29), (32), and (35), respectively. Fig. 5 presents

the absolute parts corresponding to different soliton behaviors in the xy, xz, and xt planes. Additionally, Figs. 6 and 7 illustrate the behavior of the absolute value of the soliton with respect to time. The contour plots provide a detailed overview, which helps in understanding the nature of the solution and how the function behaves in the xy-plane. By selecting different values of y, the corresponding two-dimensional wave propagation along the x-axis is shown. In Figs. 8 and 9, we have illustrated the collisions between the lump, periodic, and solitary wave solutions of equations (39) and (42), respectively. Fig. 10 illustrates the collision of the breather and lump wave solutions of equation (46). Using time variation, the absolute solutions change their positions, which are represented as a 3D profile with a density plot and a 2D wave profile.

6 Analysis of bifurcations and equilibrium states

This section considers the following wave transformations, with an emphasis on the equilibrium and bifurcation analysis of the KDKK and BK equations (1):

$$u = W(\xi), \quad \xi = \sigma x + \tau y + \mu z - \rho t, \tag{47}$$

where σ, τ, μ, and ρ are free parameters. Inserting equation (47) into equation (1), which leads to the ordinary differential equation

$$\frac{d^2}{d\xi^2}W(\xi) + \left(\frac{\sigma\kappa_4 + \tau\kappa_5 + \mu\kappa_6 - \rho\kappa_1}{(\tau\kappa_3 + \mu\kappa_2)\,\sigma^2}\right)W(\xi) + \left(\frac{3\sigma\mu\kappa_3 + 3\tau^2\kappa_3 + 6\kappa_2\mu\tau}{2\,(\tau\kappa_3 + \mu\kappa_2)\,\sigma^2\tau}\right)\Big(W(\xi)\Big)^2 = 0. \tag{48}$$

Now, from equation (48), we get

$$\frac{d^2}{d\xi^2}W(\xi) + \chi_1 W(\xi) + \chi_2\Big(W(\xi)\Big)^2 = 0, \tag{49}$$

where $\chi_1 = \frac{\sigma\kappa_4+\tau\kappa_5+\mu\kappa_6-\rho\kappa_1}{(\tau\kappa_3+\mu\kappa_2)\sigma^2}$ and $\chi_2 = \frac{3\sigma\mu\kappa_3+3\tau^2\kappa_3+6\kappa_2\mu\tau}{2(\tau\kappa_3+\mu\kappa_2)\sigma^2\tau}$.

To obtain the two-dimensional dynamic structure, rewrite equation (49) in the form:

$$\begin{aligned} \frac{d}{d\xi}W(\xi) &= Y(\xi), \\ \frac{d}{d\xi}Y(\xi) &= -\chi_1 W(\xi) - \chi_2\Big(W(\xi)\Big)^2. \end{aligned} \tag{50}$$

In this case, the Hamiltonian function $H = H(W,Y)$ associated with the solution of the dynamic system (50), we can write

$$H = \frac{1}{2}Y^2 + \frac{\chi_1}{2}W^2 + \frac{\chi_2}{3}W^3. \tag{51}$$

The total energy of a dynamical system is denoted by H, which is the sum of the potential and kinetic energies of the particles, and it depends on their position and momentum. The paths along which the total energy remains constant are shown visually. Equation (51) satisfies $\frac{dW}{d\xi} = \frac{\partial H}{\partial Y}$ and $\frac{dY}{d\xi} = -\frac{\partial H}{\partial W}$. For the dynamic system (50), if $\frac{dW}{d\xi} = 0$ and $\frac{dY}{d\xi} = 0$, then the equilibrium points (EPs) are $(0,0)$ and $(-\frac{\chi_1}{\chi_2},0)$. Let Tr and D be the trace and determinant of the Jacobian matrix (JM). Then, we can write:

$$JM = \begin{bmatrix} 0 & 1 \\ -\chi_1 - 2\chi_2 W & 0 \end{bmatrix}, \quad Tr = 0, \quad D = \chi_1 + 2\chi_2 W. \tag{52}$$

From the theory of planner dynamical systems, we can write the critical points of system (50) as follows: if $D < 0$ ($D > 0$), then EP is a saddle point (center), and if $D = 0$, then EP is a zero point. The eigenvalues of

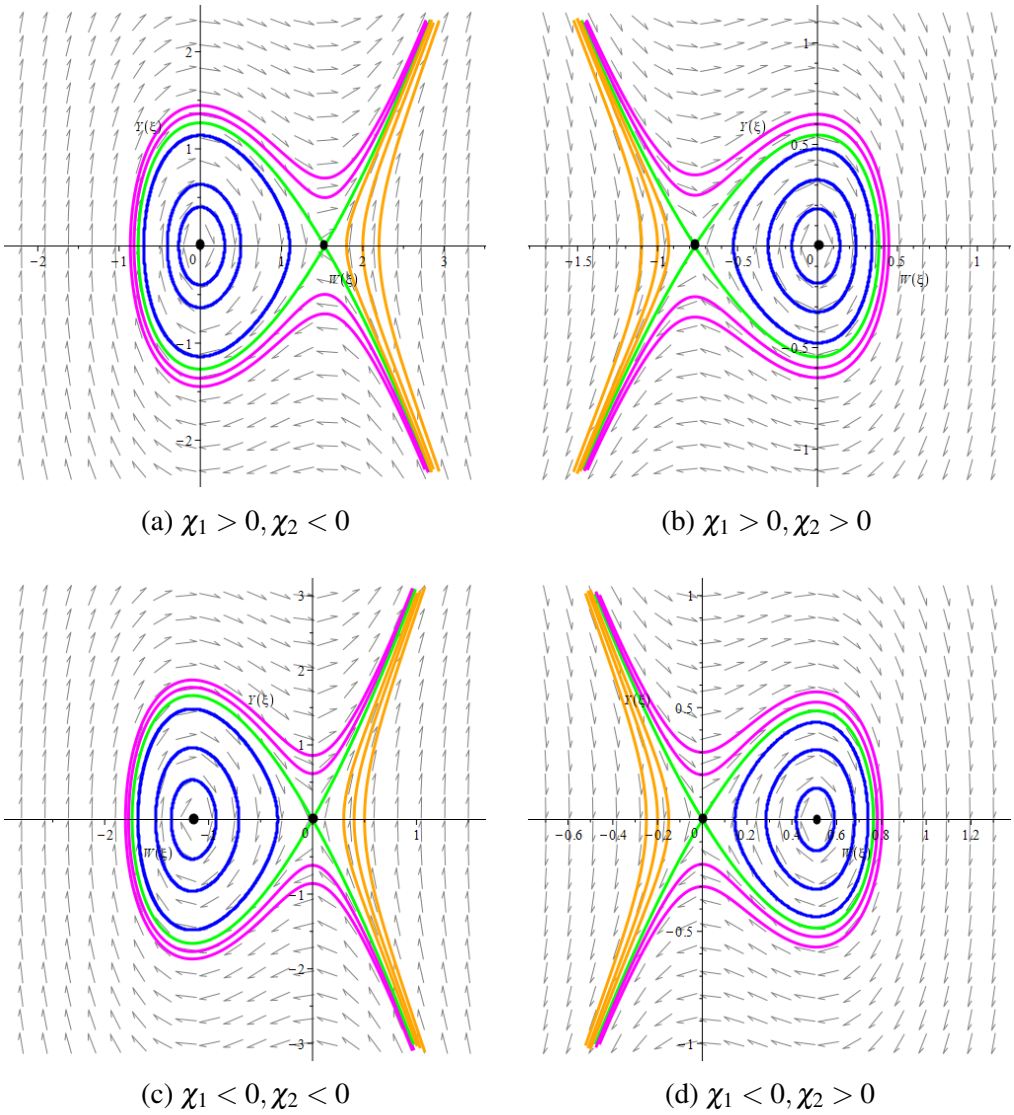

(a) $\chi_1 > 0, \chi_2 < 0$ (b) $\chi_1 > 0, \chi_2 > 0$

(c) $\chi_1 < 0, \chi_2 < 0$ (d) $\chi_1 < 0, \chi_2 > 0$

Fig. 11 Phase portrait graph of the dynamic system (50) using different parameter values.

the dynamic system are $\lambda = \pm\sqrt{-\chi_1 - 2\chi_2 W}$. We first study the EPs to investigate the phase portraits of the dynamical system (50). For $(0,0)$, the eigenvalues are $\lambda = \pm\sqrt{-\chi_1}$, whereas $\lambda = \pm\sqrt{\chi_1}$ are eigenvalues for the EP $(-\frac{\chi_1}{\chi_2}, 0)$. It is easily seen that if $\chi_1 \neq 0$, then the system (50) has two EPs, $(0,0)$ and $(-\frac{\chi_1}{\chi_2}, 0)$. Meanwhile, if $\chi_1 = 0$, then the system (50) has only one EP $(0,0)$. All the equilibrium points lie on the W-axis. The study of dynamical systems involves four distinct phenomena, namely:

Case I. $\chi_1 > 0$, $\chi_2 < 0$

In this case, the EPs $(0,0)$ and $(-\frac{\chi_1}{\chi_2}, 0)$ are the center and saddle point, respectively. Fig. 11a shows the phase portrait graph of the dynamic system (50) with free parameters. Here, the two extended curves of a homoclinic orbit are shown in green. There are two types of orbits in this family: the first type, shown in blue, consists of various periodic trajectories that rotate clockwise around the center point $(0,0)$. The second type is a family of orbits that have a hyperbolic shape, highlighted in orange. Additionally, the homoclinic orbits are highlighted in magenta, representing the only remaining members of this family of orbits. Fig. 12 shows the Hamiltonian function of the dynamic system (51) through 2D, 3D, and contour graphics.

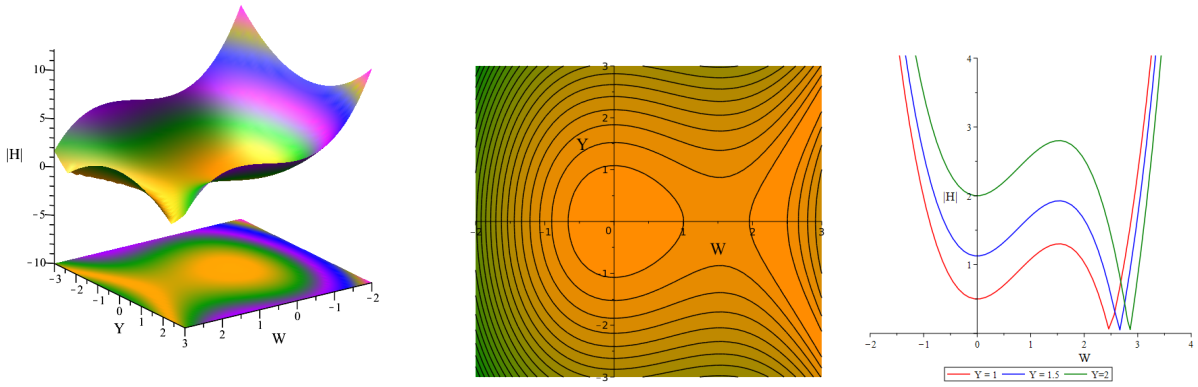

(a) (b) (c)

Fig. 12 Hamiltonian function graphics for the dynamical system (51) for $\kappa_1 = 0.3$, $\kappa_2 = 0.5$, $\kappa_3 = 0.8$, $\kappa_4 = 0.8$, $\kappa_5 = 0.5$, $\kappa_6 = 0.3$, $\sigma = 1.2$, $\tau = 1.1$, $\mu = -0.8$, and $\rho = -0.5$.

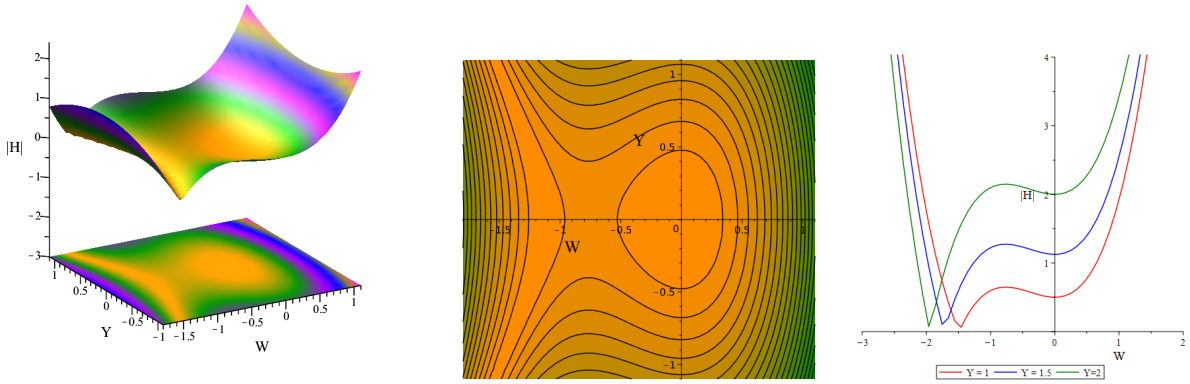

(a) (b) (c)

Fig. 13 Hamiltonian function graphics for the dynamical system (51) for $\kappa_1 = 0.3$, $\kappa_2 = 0.5$, $\kappa_3 = 0.3$, $\kappa_4 = 0.8$, $\kappa_5 = 0.5$, $\kappa_6 = 0.3$, $\sigma = 1.2$, $\tau = 1.1$, $\mu = 0.8$, and $\rho = 0.5$.

Case II. $\chi_1 > 0$, $\chi_2 > 0$

In this case, the EPs $(0,0)$ and $(-\frac{\chi_1}{\chi_2},0)$ are the center and saddle point, respectively. Fig. 11b shows the phase portrait graph of the dynamic system (50) using the free parameters. Fig. 13 shows a graphical representation of the Hamiltonian function of system (51), including 2D, 3D, and contour plots. The discussion is similar to the previous Case I, which applies to both Figs. 11b and 13.

Case III. $\chi_1 < 0$, $\chi_2 < 0$

In this case, the EPs $(0,0)$ and $(-\frac{\chi_1}{\chi_2},0)$ are the saddle and center points, respectively. Fig. 11c shows the phase portrait graph of the dynamic system (50) with free parameters. Here, the two extended curves of a homoclinic orbit are shown in green. There are two types of orbits in this family: the first type, shown in blue, consists of various periodic trajectories that rotate clockwise around the center point $(-\frac{\chi_1}{\chi_2},0)$. The second type is a family of orbits that have a hyperbolic shape, highlighted in orange. Additionally, the homoclinic orbits are highlighted in magenta, which are the only remaining members of this family of orbits. Fig. 14 shows the

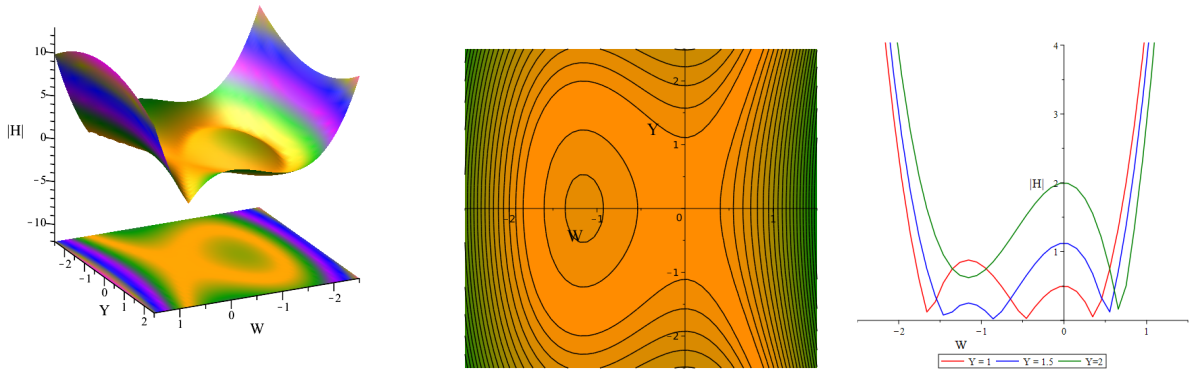

(a) (b) (c)

Fig. 14 Hamiltonian function graphics for the dynamical system (51) for $\kappa_1 = 0.3$, $\kappa_2 = -0.5$, $\kappa_3 = 0.8$, $\kappa_4 = 0.8$, $\kappa_5 = -0.5$, $\kappa_6 = 0.3$, $\sigma = 0.9$, $\tau = -0.5$, $\mu = -0.4$, and $\rho = -0.5$.

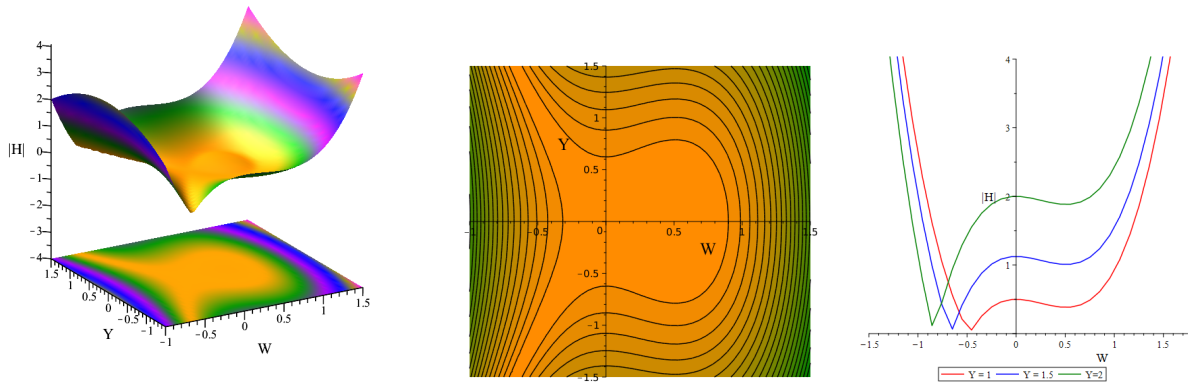

(a) (b) (c)

Fig. 15 Hamiltonian function graphics for the dynamical system (51) for $\kappa_1 = 0.3$, $\kappa_2 = 0.5$, $\kappa_3 = 0.8$, $\kappa_4 = 0.8$, $\kappa_5 = 0.5$, $\kappa_6 = 0.3$, $\sigma = -0.9$, $\tau = 0.5$, $\mu = -0.4$, and $\rho = -0.5$.

Hamiltonian function of the dynamic system (51) through 2D, 3D, and contour graphics.

Case IV. $\chi_1 < 0$, $\chi_2 > 0$

In this case, the EPs $(0,0)$ and $(-\frac{\chi_1}{\chi_2},0)$ are the saddle and center points. Fig. 11d shows the phase portrait graph of the dynamic system (50) using the free parameters. Fig. 15 shows a visual representation of the Hamiltonian function of system (51), including 2D, 3D, and contour plots. The discussion is similar to the previous Case III, which applies to both Figs. 11d and 15.

7 Analysis of sensitivity

In this section, the dynamics of the KDKK and BK equations (1) are examined to see how small changes in parameters or initial conditions affect the behavior of a dynamic system. We analyze the sensitivity of the dynamic system (50) by utilizing the Runge-Kutta technique. The parameters $\kappa_1 = 0.3$, $\kappa_2 = 0.5$, $\kappa_3 = 0.8$, $\kappa_4 =$

0.8, $\kappa_5 = 0.5$, $\kappa_6 = 0.3$, $\sigma = 1.2$, $\tau = 1.1$, $\mu = -0.8$, and $\rho = -0.5$ are chosen to solve this system. To investigate the sensitivity of the system, we also consider four different initial conditions: IC1 $[W(0) = 0.12, Y(0) = 0]$; IC2 $[W(0) = 0, Y(0) = 0.12]$; IC3 $[W(0) = 0.22, Y(0) = 0]$; and IC4 $[W(0) = 0, Y(0) = 0.22]$.

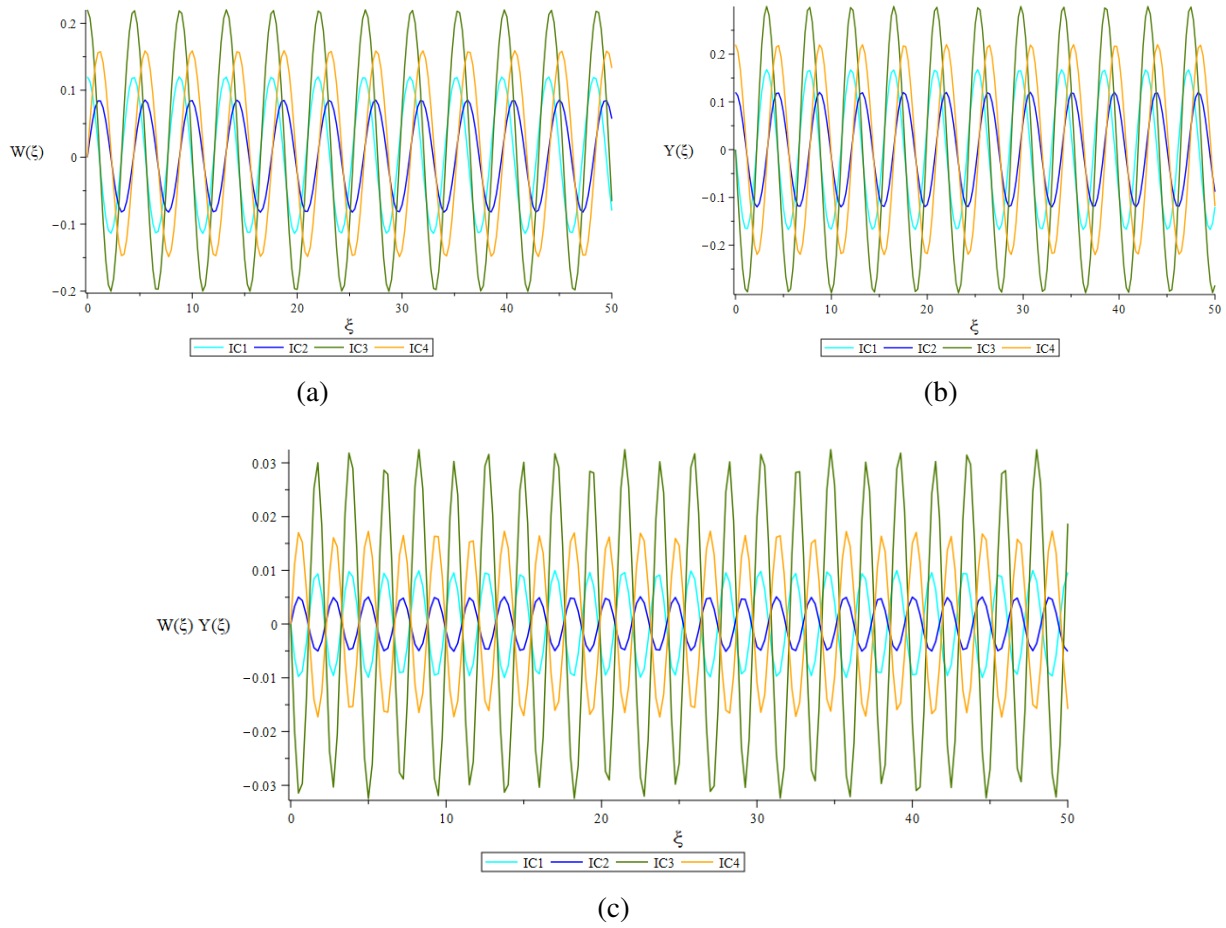

Fig. 16 Sensitivity analysis of the dynamical system (50) with different initial conditions.

Additionally, Fig. 16 demonstrates the consistency of the unperturbed system (50) and analyzes how the system behaves under different initial conditions. This figure illustrates the sensitivity analysis of $W(\xi)$, $Y(\xi)$, and $W(\xi)\,Y(\xi)$ with respect to ξ, based on four distinct initial conditions. Fig. 16 shows four colors: cyan, blue, leaf green, and orange. Here, the cyan curve represents IC1 (0.12, 0), the blue curve represents IC2 (0, 0.12), the leaf green curve represents IC3 (0.22, 0), and the orange curve represents IC4 (0, 0.22), respectively. Leaf green indicates a long height curve, while blue indicates a short height curve. The graphs highlight the complex structure and variations of the system, making it easier to show how the system has changed over time under different initial conditions. Even small changes in the initial conditions can considerably affect the system's behavior. Therefore, we identify that a minimum sensitivity is present in the given equation.

8 Conclusion

In this work, we applied the Hirota bilinear technique to determine the bilinear form of a generalized (3+1)-dimensional KDKK and BK equation that identifies the physical phenomenon of the waveform. Using a

computer program known as Maple software, we illustrate the characteristics of collisions between different waves. The dynamical behaviour of lump waves and their collisions with single-lump and solitary waves, lump and periodic waves, and lump and breather waves has been examined and described using various ansatz functions. In addition, we illustrate how the lump interacts with breather waves, periodic waves, and solitary waves to generate different types of dynamical patterns in the solutions. The nature of the solutions is displayed visually, including 2D, 3D, and contour graphics. Figs. 1 and 2 show the dynamic structure and features of the lump wave solutions, whereas Figs. 3-10 display all the collisions between various waves. Also, the bifurcation process and sensitivity analysis of dynamic structures are studied based on the theory of planar dynamical systems. The exact stable Hamiltonian system is derived using a well-known Galilean transformation. We also demonstrate the phase diagram while performing a qualitative analysis of the Hamiltonian function. Therefore, the obtained results will help in understanding and describing the complex physical structure and characteristics of wave profiles related to fluid mechanics, shallow water waves, nonlinear dynamics, and ocean engineering. The advanced method proposed here can be easily applied to other nonlinear higher-dimensional systems, opening up new possibilities for studying wave-structure interactions in various computational engineering, optical fibers, nonlinear sciences, and other advanced scientific domains. In the future, researchers can extend the current research to multi-dimensional nonlinear mathematical models that include numerous physical parameters, and also investigate turbulent wave systems that more closely resemble real-world fluid dynamics and nonlinear dynamics.

9 Declarations

9.1 Conflict of interest:

The authors declare that they have no conflict of interest.

9.2 Funding:

Not applicable.

9.3 Author's contribution:

S.K.- Conceptualization, Validation, Investigation, Supervision, Writing-Original Draft. J.K.- Formal Analysis, Software, Methodology, Visualization, Writing-Review, Editing. All authors read and approved the final submitted version of this manuscript.

9.4 Acknowledgement:

The authors would like to sincerely thank the Editor and the reviewers for their insightful comments and valuable suggestions, which have significantly improved the quality of the manuscript. Sachin Kumar also wishes to acknowledge the financial support provided by the Institution of Eminence, University of Delhi, India, through the Faculty Research Programme Grant under the IoE Scheme, with Reference No. IoE/2025-26/12/FRP.

9.5 Data availability statement:

All data that support the findings of this study are included within the article.

9.6 Usage of AI tools:

The authors declare that they have not used Artificial Intelligence (AI) tools in the creation of this article.

References

[1] Alharbi A.F., Akram U., Ansatz-based exploration of M-shaped and multi-wave solitons in the Kudryashov-Sinelshchikov model, Modern Physics Letters B, 39(29), 2550169, 2025.
[2] Hamid I., Kumar S., Newly formed solitary wave solutions and other solitons to the (3+1)-dimensional mKdV-ZK equation utilizing a new modified Sardar sub-equation approach, Modern Physics Letters B, 39(18), 2550027, 2025.
[3] Günay B., Optical soliton solutions to a higher-order nonlinear Schrödinger equation with Kerr law nonlinearity, Results in Physics, 27, 104515, 2021.
[4] Gunasekar T., Raghavendran P., Santra S.S., Majumder D., Baleanu D., Balasundaram H., Application of Laplace transform to solve fractional integro-differential equations, Journal of Mathematics and Computer Science, 33(3), 225–237, 2024.
[5] Ma W.X., Zhou Y., Lump solutions to nonlinear partial differential equations via Hirota bilinear forms, Journal of Differential Equations, 264(4), 2633–2659, 2018.
[6] Yu J.P., Sun Y.L., Study of lump solutions to dimensionally reduced generalized KP equations, Nonlinear Dynamics, 87(4), 2755–2763, 2017.
[7] Manakov S.V., Zakharov V.E., Bordag L.A., Its A.R., Matveev V.B., Two-dimensional solitons of the Kadomtsev-Petviashvili equation and their interaction, Physics Letters A, 63(3), 205–206, 1977.
[8] Kharif C., Pelinovsky E., Slunyaev A., Rogue Waves in the Ocean, Springer, USA, 2008.
[9] Alshammari F.S., Hoque M.F., Dynamical solitary interactions between lump waves and different forms of n-solitons ($n \to \infty$) for the (2+1)-dimensional shallow water wave equation, Partial Differential Equations in Applied Mathematics, 3, 100026, 2021.
[10] Stenflo L., Marklund M., Rogue waves in the atmosphere, Journal of Plasma Physics, 76(3-4), 293–295, 2010.
[11] Li B.Q., Ma Y.L., Rogue waves for the optical fiber system with variable coefficients, Optik, 158, 177–184, 2018.
[12] Tan W., Dai Z.D., Xie J., Qiu D.Q., Parameter limit method and its application in the (4+1)-dimensional Fokas equation, Computers and Mathematics with Applications, 75(12), 4214–4220, 2018.
[13] Zhang R.F., Li M.C., Cherraf A., Vadyala S.R., The interference wave and the bright and dark soliton for two integro-differential equation by using BNNM, Nonlinear Dynamics, 111(9), 8637–8646, 2023.
[14] Yang D., Dynamic properties of soliton solutions for the generalized KDKK and BK equations, The European Physical Journal Plus, 140(3), 255, 2025.
[15] Hirota R., The Direct Method in Soliton Theory, Cambridge University Press, UK, 2004.
[16] Li S., Li L., Painlevé integrability, Auto-Bäcklund transformation and exact solutions of an extended (3+1)-dimensional Boussinesq equation, Qualitative Theory of Dynamical Systems, 24(3), 110, 2025.
[17] Matveev V.B., Salle M.A., Darboux Transformations and Solitons, Springer, Germany, 1992.
[18] Guan X., Liu W., Zhou Q., Biswas A., Darboux transformation and analytic solutions for a generalized super-NLS-mKdV equation, Nonlinear Dynamics, 98(2), 1491–1500, 2019.
[19] Feng Y., Zhao Z., New lump solutions and several interaction solutions and their dynamics of a generalized (3+1)-dimensional nonlinear differential equation, Communications in Theoretical Physics, 76(2), 025001, 2024.
[20] Chen W., Tang L., Tian L., Lump, breather and interaction solutions to the (3+1)-dimensional generalized Camassa-Holm Kadomtsev-Petviashvili equation, Journal of Mathematical Analysis and Applications, 526(2), 127275, 2023.
[21] Ma W.X., Manukure S., Wang H., Batwa S., Lump solutions to a (2+1)-dimensional fourth-order nonlinear PDE possessing a Hirota bilinear form, Modern Physics Letters B, 35(09), 2150160, 2021.
[22] Wang M., Tian B., Sun Y., Zhang Z., Lump, mixed lump-stripe and rogue wave-stripe solutions of a (3+1)-dimensional nonlinear wave equation for a liquid with gas bubbles, Computers and Mathematics with Applications, 79(3), 576–587, 2020.
[23] Yang J.Y., Ma W.X., Lump solutions to the BKP equation by symbolic computation, International Journal of Modern Physics B, 30(28n29), 1640028, 2016.
[24] He C., Tang Y., Ma W.X., Ma J., Interaction phenomena between a lump and other multi-solitons for the (2+1)-dimensional BLMP and Ito equations, Nonlinear Dynamics, 95, 29–42, 2019.
[25] Zhou Y., Zhang X., Zhang C., Jia J., Ma W.X., New lump solutions to a (3+1)-dimensional generalized Calogero-Bogoyavlenskii-Schiff equation, Applied Mathematics Letters, 141, 108598, 2023.
[26] Miles J.W., The Korteweg-de Vries equation: A historical essay, Journal of Fluid Mechanics, 106, 131–147, 1981.
[27] Li Y., Yao R., Xia Y., Molecules and new interactional structures for a (2+1)-dimensional generalized Konopelchenko-Dubrovsky-Kaup-Kupershmidt equation, Acta Mathematica Scientia, 43(1), 80–96, 2023.
[28] Chen S.T., Ma W.X., Lump solutions to a generalized Bogoyavlensky-Konopelchenko equation, Frontiers of Mathematics in China, 13, 525–534, 2018.
[29] Elbrolosy M.E., Elmandouh A.A., Dynamical behaviour of nondissipative double dispersive microstrain wave in the microstructured solids, The European Physical Journal Plus, 136(9), 955, 2021.
[30] Kumar S., Mann N., Kharbanda H., Inc M., Dynamical behavior of analytical soliton solutions, bifurcation analysis, and quasi-periodic solution to the (2+1)-dimensional Konopelchenko-Dubrovsky (KD) system, Analysis and

Mathematical Physics, 13(3), 40, 2023.
[31] Kumar S., Mann N., Dynamic study of qualitative analysis, traveling waves, solitons, bifurcation, quasiperiodic, and chaotic behavior of integrable Kuralay equations, Optical and Quantum Electronics, 56(5), 859, 2024.
[32] Kumar S., Rani S., Mann N., Analytical soliton solutions to a (2+1)-dimensional variable coefficients Graphene Sheets equation using the application of Lie symmetry approach: Bifurcation theory, sensitivity analysis and chaotic behavior, Qualitative Theory of Dynamical Systems, 24(2), 80, 2025.
[33] Song Y., Yang B., Wang Z., Bifurcations and exact solutions of a new (3+1)-dimensional Kadomtsev-Petvíashvili equation, Physics Letters A, 461, 128647, 2023.
[34] Kumar S., Mohan B., Kumar R., Newly formed center-controlled rouge wave and lump solutions of a generalized (3+1)-dimensional KdV-BBM equation via symbolic computation approach, Physica Scripta, 98(8), 085237, 2023.
[35] Wazwaz A.M., Painlevé integrability and lump solutions for two extended (3+1)-and (2+1)-dimensional Kadomtsev-Petviashvili equations, Nonlinear Dynamics, 111(4), 3623–3632, 2023.
[36] Weiss J., Tabor M., Carnevale G., The Painlevé property for partial differential equations, Journal of Mathematical Physics, 24(3), 522–526, 1983.